ISSN: 3068-2789

Review Article

Journal of All Physics Research and Applications

Macroscopic Properties of the Strong Interaction

Plekhanov VG*

Fonoriton Sci. Lab., Garon Ltd., Tallinn, Estonia

***Corresponding author:**
Plekhanov VG, *Fonoriton Sci. Lab., Garon Ltd., Tallinn, Estonia*.

Abstract
The measured isotopic shift of the zero - phonon emission line of free excitons in low - temperature (2 K) spectra of intrinsic luminescence of LiD crystals made it possible for the first time to obtain not only the value of the neutron - electron binding energy, but also its dependence on the distance between the proton and neutron in the deuterium nucleus. The obtained nonlinear dependence of the strong interaction coupling constant on the neutron - electron binding energy is associated with the manifestation of a new force in the mass isotope effect, previously not observed. The isotopic open of a band - gap in graphene proves that mass is created in massless fermions (leptons) in graphene by the strong nuclear interaction. The need for further theoretical investigation of nucleon dynamics in nuclear physics is emphasized.

Keywords: Strong Interaction, Hadrons, Quarks, Gluons, Excitons, Phonons, QED, QCD.

Received: February 12, 2026;
Accepted: February 19, 2026;
Published: February 26, 2026

PACS

112.38-t; 12.39-x; 14.20-o; 78.55 Hx

Introduction

Simple atoms, like hydrogen, being essentially quantum electrodynamics (QED) systems, allow highly accurate theoretical predictions. QED is the first successful and still the most successful quantum field theory. The spectacular success of QED gives physicists great confidence in Maxwell's equation on the one hand and Dirac's equation on the other, yet something is missing in relations between them [1]. After the discovery of the neutron in 1932 by Chadwick, there was no longer doubt that the building block of nuclei are proton and neutron (collectively called nucleons). The discovery of the neutron may be viewed as the birth of the strong nuclear interaction: it indicated that the nuclei consist of protons and neutrons and hence the presence of a force that holds them together, strong enough to counteract the electromagnetic repulsion. Theory strong nuclear interaction is the heart of quantum chromodynamics (QCD) which is part of the Standard Model (SM), therefore the base exchange is the gluon which mediates the forces between quarks [2,3]. Nucleus is a bound system of strongly interacting protons and neutrons (more generally baryons and mesons - this is the reason for the collective name hadrons) holds atomic nuclei together and, in another context, binds quarks within hadrons. The baryons are bound states of the three quarks and mesons are composed of quark and antiquark [4].

The subject of elementary particle physics to have begun with the discovery of the electron more than century ago. In the following 50 years, one new particle after another was discovered, mostly as a result of experiments with cosmic rays, the only source of very high energy particle then available. After second war the accelerator technique was used to study the elementary particle physics. Nuclear and particle physics are essentially at the forefront of nowadays understanding of physics. Nucleus is a bound system of strongly interacting protons and neutrons.

Citation: Plekhanov VG (2026) Macroscopic Properties of the Strong Interaction. J All Phy Res Appli 2: 1-18.

Unfortunately, modern Quantum Electrodynamics (QED) does not provide us with the tools to calculate the bound states properties of the proton (deuteron) from first principles [1]. The present review is devoted to the results of measurements of residual strong nuclear interaction via the study the low - temperature optical spectra (reflection, photoluminescence) of the LiH (without strong interaction in hydrogen nucleus) and LiD (with strong interaction in deuterium nucleus) crystals which are different by term of one neutron from each other as well as very rich of diamond allotropes (diamond, graphite, graphene, fullerene). We should repeat that nowadays in text books and elsewhere the separation of electromagnetic and strong interaction is tacitly assumed. It is very strange because up to present time we do not even know the strong nuclear force very well. The origin of the strong interaction is very important especially in the problem of all force unification [5]. The results of the paper have shown a new light on some residual strong nuclear interaction (ultimately based in the character of magnetic forces, the electromagnetic or color origin, which by their very nature, are difficult to conceal within the elusive nucleon physical boundary) between both kind of forces which experimentally manifested through isotopic shift of zero phonon line in optical spectra [6].

As indicated above, there is a common place in Standard Model (SM) of modern physics; that the strong force does not act on leptons [5]. Following this conclusion we do not must to observe the dependence of the optical properties of solids on addition neutrons in substance. This contradicts the history of the development of isotope effect. The first attempt to discover an interaction between neutrons and electrons was made by Dee in the same year, 1932 in which the neutron was discovered by Chadwick [7,8]. In 1936, Condon pointed out that the existence of a neutron - electron interaction would give rise to an isotope shift in spectral lines of atoms, which was observed for the first time by Aronberg in 1918 in the line spectra of Pb isotopes (see, also review [9-11]. The existence of a weak attractive interaction between electrons and neutrons has been described in the series papers by Foldy [12]. Foldy has showed that neutron - electron interaction has two contributions - one arising from anomalous magnetic moment of the neutron and the other from an intrinsic Darwin coefficient - electric field. This picture was justifiable in meson theory though both of these contributions have a common origin [5,12-14]. In all methods of the measurements there are principal troubles connected with the necessity of introducing large corrections in size of order of the investigated effect of neutron - electron interaction. Besides there is intrigue in the fact that all known experimental values (and references quoted therein) were scattered around the so called Foldy scattering length in the interval ± 10% [14,15]. The main conclusion of the fundamental papers by Foldy is that the intrinsic neutron - electron interaction is essentially an electromagnetic interaction between the neutron and the charge density producing an external electromagnetic field by electron [12,15].

According to contemporary physics the strong force does not act on lepton (electrons, positrons, muons and neutrinos), but only on protons and neutrons (more generally, on baryons and mesons - this is the reason for the collective name hadrons) (see, however below). It should be added that the forces between the quarks must be long range, because the gluons (as photons) have zero mass. This does not imply that the forces between hadrons are also long - range, because hadrons have zero color charges overall. The forces between the colorless hadrons are the residues of the for as between their quark constituents, and cancel when the hadrons are far apart [2-4]. In 1935, Yukawa pointed out that the nuclear force could be generated by the exchange of a hypothetical spinless particle, provided its mass intermediate between the masses of proton and electron - a meson [17]. Yukawa predicted the pion [1-4]. The macroscopic manifestations of the strong interaction are restricted up to know to radioactivity and the release of nuclear energy. Yutaka's potential has the form

$$V = g\frac{e^{-kr}}{r^n}, \qquad (1)$$

for some n. Here the strength of the force is measured by the constant k [5]. The most important feature Yukawa's forces are that they have a small range (~ 10^{-15}m). The central dogma of atomic physics after Yukawa's paper that proton - electron attraction could be explained in terms of classical electrostatic theory, while the strong force effects were essentially new and inexplicable. So, far the best theoretical guess is the Yukawa potential, but it is a static potential not dependent on velocities of the nucleons. A static force is not a complete one because it cannot explain the propagation of the nuclear interaction. Moreover, as was indicated above, a phenomenological Yukawa potential cannot be directly verified experimentally. We should note that nowadays in text books and elsewhere the separation of electromagnetic and strong interaction tacitly assumed. It is very strange up to present time we do not even know the strong force very well. And what is more we having some contradiction taking into account that the forces between quarks must be long - range, because the gluons have zero mass. But as was mentioned above the force between colorless hadrons is short - range, when the distance between hadrons is more than nuclear size [1,17,18].

One may consider four families of particles in order of increasing rest mass; the first contains only one member, the proton, a boson of spin 1. The second family, leptons, contains fermions of spin 1/2, lighter than proton. Leptons are subject to electromagnetic and Fermi interaction only, not the strong interaction (see however below). The third family, mesons, comprises bosons of spin 0. These are heavier than the leptons, lighter than the protons, and the subject to all three types of interactions; weak, strong and electromagnetic. The fourth family, baryons, comprises the proton and heavier fermions. Baryons are subject to all three types of interactions; those heavier than neutron is called hyperons.

Table 1: The four fundamental forces.

Interaction TTS(s)	FQ	Mass	Range (m)	RS	Spin	TC-S (m2)
Str 10^{-23}	Gluon	0	10^{-15}	1	1	10^{-30}
We 10^{-8}	W , Z	81, 93 GeV/c2	10^{-18}	10^{-5}	1, 1	10^{-44}
Elec 10^{-20}	Photon	0	∞	1/137	1	10^{-33}
Gra	Graviton	0	∞	10^{-38} 2	-	-

Here - FQ field quant, RS relative strength, TC - S Typical cross - section, TTS - Typical time scale.

The Table 1 given for the strength and range of the forces come from a comparison of the effects they produce on two protons [19]. In some respect these resemble an ordinary Newtonian force between the protons, varying with the distance between them as if the force was derived from a potential function (1): for some n. This is an inverse - power force which is diminished by an exponential factor at distances larger than a certain distance R, the range of the force. The strength of the force is measured by the constant k. The unit of strength is hc/2л where h is Planck's constant and c the speed of light. Thus, nuclear physics was essentially the paradigmatic example of understanding particle physics. The modern quantomechanical view of the three fundamental forces (all except gravity) is that particles of matter (fermions neutrons, protons, electrons) do not directly interact with each other, but rather carry a charge, and exchange virtual particles (gauge bosons photons, gluons, gravitons) which are the interaction carriers or force mediators. As can be seen from Table 1, photons are the mediators of the interaction of electric charges (protons, electrons, positrons); and gluons are the mediators of the interaction of color charges (quarks). In our days, the accepted view is that all matter is made of quarks and leptons. As can be seen, of the three pairs of quarks and leptons, one pair of each - the quark u and d and the leptons e and v_e (electrons neutrino) - are necessary to make up the everyday world, and a world which contained only these would seem to be quite possible.

As we can see above the method of the scattering particles allows to determine only length of scattering as well as the size and depth (highest) of the neutron's potential. In the present paper we attempt to measure the energy of the neutron - electron interaction via spectroscopic study of the optical characteristics of solids with isotope effect at low temperature. Therefore, it is purpose of our paper to advance a description of the manifestation of strong nuclear interaction in solids, using partly published and new non - accelerator experimental results. Our spectroscopic measurement of the low temperature optical characteristics of LiH_xD_{1-x} crystals is permitted to quantitative study of the dependence of strong coupling constant, αs, on the proton - neutron distance in the deuteron nuclei. Carbon, being the second element after silicon on Earth, has unusually wide range of allotropic compounds with completely different physical properties [20]. The use of our object allows the investigation of not only the isotope effects in lattice dynamics (vibrational, elastic and thermal properties), but also the influence of such effects on the electronic excitations (for example, the renormalization of the band - to - band transition energy E_g). We emphasize that the study of the isotope effect remains at the forefront not only in materials science, but also nuclear and high energy physics.

Isotopically pure materials represent a separate class of modern materials science, which is an accelerator of the development of the latest fine technology. First of all, it is necessary to remember due to this explosive leap in the development of electronic and optical technologies. It is thanks to isotopically pure silicon used in personal computer processors that it has been possible to step beyond the 3GHz threshold. Moreover, isotopically pure germanium is the best weak signal detector. Low dimensional structures of quantum wires (QW), quantum dots (QD) received a new impetus for development when using isotopically pure materials, as well as artificially regulating the isotopic composition of a material. We emphasize that due to the wide class of allotropic carbon compounds, the physical properties of which vary from transparent in the ultraviolet (UV) range (diamond) to opaque (graphite, graphene), from dielectric (diamond) to a compound with metallic conductivity (graphene) and also which have extremely different elastic and thermal properties - all of the above-mentioned characteristics exhibit isotopic dependence. We must substitute ^{12}C for a heavy isotope ^{13}C. Semiconductor graphene could come to replace all silicon electronics. Of course, the new technology for the development of quantum computer (QC) processors is based on the use of materials with different spin values. Great demand for isotopically pure materials from control agencies. For example, a special requirement for isotopically pure silicon, from which it is planned to make a control sample of 1 kg. We will not at all touch upon the very wide applications of pure isotopes in biophysics and medicine. As an example, let us point out that only one country (USA) uses tens of thousands of tons of different isotopes per year.

The present paper reviews of recent research work on the preparation and remarkable properties of isotope - mixed systems, covering wide range of topics from physics of elementary particles, materials science to engineering applications, including in quantum information and quantum computers. Artificial activation of the strong interaction by adding of one neutron to the nucleus causes the global reconstruction of the macroscopic characteristics of solids. The experimental evidence of macroscopic manifestation of the strong interaction in optical spectra of solids which are different by term of one neutron from each other (using LiD crystals instead LiH) has been presented. The initial components of mixed crystals LiH_xD_{1-x} are LiH (no strong interaction in the hydrogen nucleus) and LiD (with strong interaction in the deuterium nucleus) crystals are dielectrics with cubic symmetry. The change of the concentration of deuterium in mixed crystals LiH_xD_{1-x} determines the change in the distance between nucleons, which is directly manifested in the position of the phononless free exciton emission line in the low - temperature luminescence spectrum. A series of such measurements made it possible to construct a function of the dependence of the energy of strong nuclear interaction on the distance between nucleons in the deuterium nucleus. This evidence is directly seen from luminescence (reflection) and scattering spectra. As far as the gravitation, electromagnetic and weak interactions are the same in both of kind crystals, it only emerges the strong interaction in deuterium nucleus. Therefore, a sole conclusion is made that the renormalization of the energy of electromagnetic excitations (electrons, excitons, phonons) is carried out by the strong nuclear interaction. The measurements of the dependence of the energy of strong nuclear interaction on the distance between nucleons in a nucleus were performed for the first time and these results allow to find the maximum possible value of α_s = 2.4680. Our non - accelerator results open new avenue in the investigation of the propagation the force of strong nuclear interaction in the wide value range by means the condensed matter alike traditional

accelerator methods. Carbon, being the second element after silicon on Earth, has unusually wide range of allotropic compounds with completely different physical properties. Carbon is the second sample of our investigations. The use of our object allows the investigation of not only the isotope effects in lattice dynamics (vibrational, elastic and thermal properties), but also the influence of such effects on the electronic excitations (for example, the renormalization of the band - to - band transition energy E_g). This article is a continuation on the study work of nuclear properties and processes using solid - state low - temperature spectroscopy method. We emphasize that the study of the isotope effect remains at the forefront not only in materials science, but also nuclear and high energy physics.

The discovery of global changes in macroscopic, including optics, properties upon the addition of one neutron made the unique crystals of LiH and LiD(diamond, graphene), which differ by one neutron, an excellent model for studying the strong interaction [21]. Indeed, in both crystals the lithium ions, protons and electrons are the same, and therefore the gravitational, electromagnetic and weak interaction are the same and the addition of one neutron, according to Yukawa, generates a strong interaction between the proton and the neutron in the deuterium nucleus, the influence of which on the electron (lepton) is manifested in the observed isotopic shift of zero - phonon line in low - temperature luminescence spectra of LiD crystals. We have previously emphasized the importance of using low - temperature spectroscopy to study strong nuclear interaction [1]. Let us add in this regard that a recently published sensible, informative review the author adheres to the already traditional direction of searching for new physics and the origin of mass beyond the SM boundary in high - energy physics by more powerful accelerators [24]. It is worth recalling that already in work the clarification of the origin of the observed world was linked with the nucleon mass [26]. To clarify this, it is necessary to understand the mechanism of breaking chiral symmetry (symmetry of the equations of motion due to the asymmetry of the Universe in QCD and the literature cited there) [25]. This author has shown that the breaking symmetry occurs at large distances of = 1 fermi = 10^{-15}m, and thus has no relation to high - energy experiments investigating small distances of 10^{-19} m [23,1]. Incidentally, we note that after our work on strong interaction in the mass isotope effect, a whole of works appeared devoted to the search for new physics in the isotope effect of heavy chemical elements. In other words, following us in those works, they are also trying to find a new type of boson interacting with a neutron and an electron [27-33].

This work complements the review with low - energy physics and the same time is a logical and experimental continuation of the work and is devoted to the search for new physics beyond the SM and the origin of mass [15-26]. In particular, a nonlinear dependence of the coupling constant of strong interaction on the value of the neutron - electron binding energy was obtained for the first time. It has been shown that the maximum value of the neutron - electron binding energy in a number of crystals (LiD, C, Ge, ZnO) equal = 105 meV is in good agreement with Breit's theoretical estimate obtained in electrostatic model and equal 106.7 meV [34].

Experimental Results

The observation of the mas isotopic shift of the zero - phonon emission line of free excitons in low - temperature (2 K) luminescence spectra of LiH and LiD crystals was carried out on the setup described by us repeatedly [1,35,36]. For the sake of clarity, we will briefly add that the experimental setup consisted of a home - made helium cryostat and two monochromators perpendicular each other. The optical signal (light reflected from the crystal, its luminescence, or light scattered by crystal) was recorded by a highly sensitive photon counting system with the signal stored in the memory of a personal computer. Taking into account the high hygroscopicity of the crystals under study, we developed a technique for cleaving crystals in superfluid helium in a helium cryostat bath. The crystal surface prepared in this way it possible to obtain reliable and easily reproducible results. Numerous studies have shown that the fundamental absorption edge is described by direct electron transitions in the center of the Brillouin zone with the creation of large - radius excitons [12,37-40].

The spectrum of free exciton photoluminescence of LiH crystals cleaved in superfluid helium (Figure 1) consists of a narrow zero - phonon emission line at the 4.950 eV and its broader phonon repetitions which arise due to radiated annihilation of the free excitons with the production of one to five longitudinal optical (LO) phonons [39, 1].

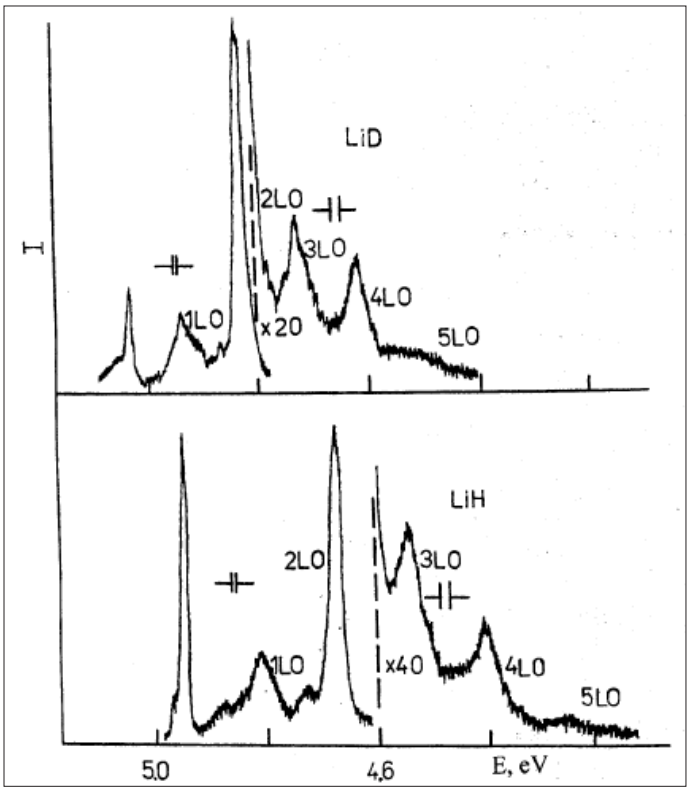

Figure 1: Photoluminescence spectra of free excitons at 2 K in LiH and LiD crystals cleaved in superfluid helium.

The phononless emission line coincides in an almost resonant way with the reflection line of exciton ground state which is indication of the direct electron transition X_1 - X_4 of the first Brillouin zone [37,39]. The lines of phonon replicas form an equidistant series biased toward lower energies from the resonance emission

line of excitons. The energy difference between these lines in LiH crystals is about 140 meV, which is very close to the calculated energy of the LO phonons in the middle of Brillouin zone [41]. Photoluminescence spectrum of LiD crystals cleaved in superfluid helium is similar in its developed structure to the given spectrum of intrinsic photoluminescence of LiH crystals.

The isotopic short - wave shift of the zero - phonon emission line of free excitons in LiD crystals, as in the case of reflection spectra, is equal to 103 meV [38]. The second change in the luminescence spectrum of LiD crystals is associated with the phonon energy, which decreased to 104 meV. The emission spectrum of free excitons in mixed crystals LiH_xD_{1-x} (Figure. 2) is in many ways similar the emission spectrum of free excitons in LiH and LiD crystals.

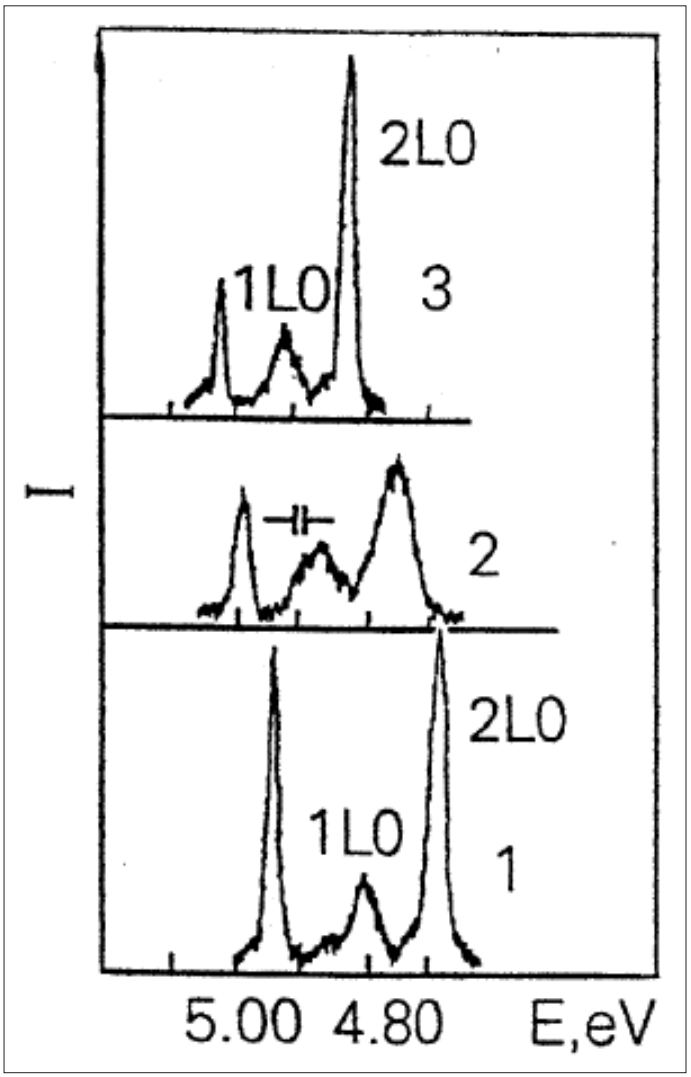

Figure 2: Photoluminescence spectra of free excitons in LiH (1), LiH_xD_{1-x} (2), and LiD (3) crystals cleaved in superfluid helium at 2 K. Spectrometer resolution is shown.

Changing the concentration of isotopes made it possible to grow (and reference quoted there) [38]. a whole range of LiH_xD_{1-x} mixed crystals. Measuring their reflection and luminescence spectra made it possible to find the energy of the zero - phonon emission line of free excitons of a whole series of crystals with different isotope concentration [39]. The results of these measurements made it possible to construct the dependence of the energy of the zero - phonon emission line of free excitons of deuterium concentration. The dependence of the lattice constant of LiH_xD_{1-x} mixed crystals on the isotope concentration, necessary for our work, was measured in paper [42]. Vegard's law is well fulfilled - the linear dependence of the crystal lattice constant on the concentration of isotopes. The obtained experimental data from the present work made it possible to construct the dependence of the energy of strong interaction (the energy of the neutron - electron bond) on the distance between the proton and the neutron in the deuterium nucleus, taking into account he linear dependence on the lattice constant on the concentration of isotopes [42]. The indicated dependence is depicted in Figure. 3, where r_D and r_H are the radii of deuterium and hydrogen nuclei according CODATA [43].

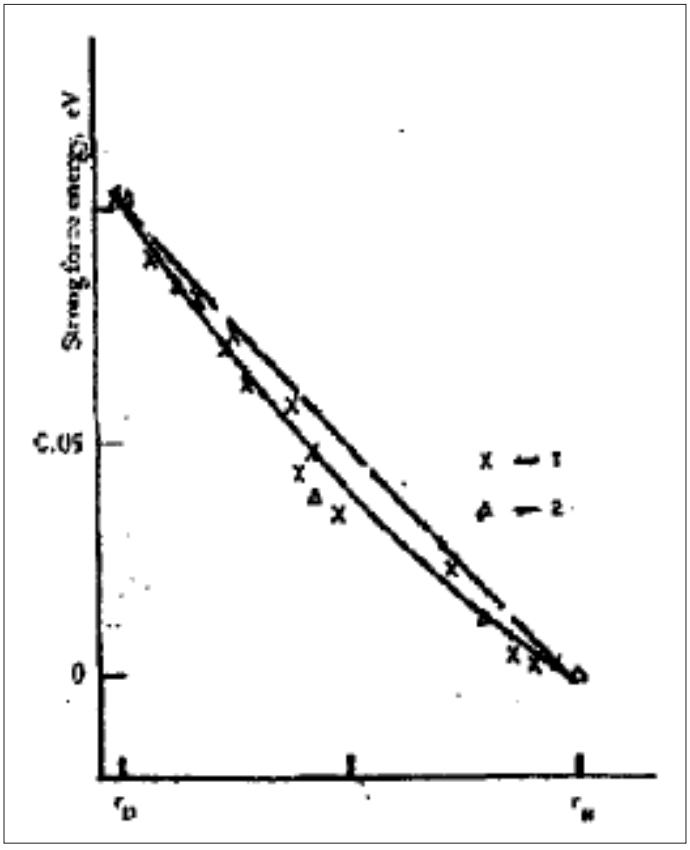

Figure 3: The long - range of the force of strong nuclear interaction dependence on the distance between nucleons in deuterium nucleus. The straight dashed line is linear dependence of the force dependence Fs in the virtual model. Points derived from reflection spectra indicated by crosses, and those from luminescence spectra by triangles

Analysis of Results and their Discussion

A) LiH Crystals

It is well known from atomic spectroscopy that the isotopic shift of spectral lines arises as a result of the shift relative to each other of the energy levels of atoms belonging to different isotopes of the same chemical elements [14]. This displacement is a result of the interaction of the electron shell with the nucleus. Therefore, the isotopic effect should manifest both the properties of the nucleus and the characteristic features of the electron shell. As noted earlier, the phenomenologically mass isotopic

shift is caused by the correction of the kinetic energy of the atomic electrons by the motion of the nucleus and is described by formula $E = \frac{1}{2}(\frac{1}{m_e} + \frac{1}{M})\sum_i p_i^2 + \frac{1}{M}\sum_{i \neq j} p_i p_j$.

Here m_e and M are the mass of the electron and the nucleus, p_i and p_j are the momenta of the i - th and j - th electrons. It is the first term of last relation that describes the isotopic shift in light elements. The second term describes the specific mass isotope shift and is due to the electron's interaction [18]. Quantum - mechanically, this interaction is described by the electron - phonon model [47]. The quantum mechanical solution to the task of electron - phonon interaction (in our case, neutron - electron interaction) is found taking into account the adiabatic approximation, which takes into account that mass of an electron is approximately 2000 times less than the mass of a nucleus [46]. The latter allows the use of perturbation theory.

The use of the adiabatic approximation leads to the appearance of non - adiabatic term, which is neglected due to its smallness (see formula 5 in [42,46]. It is precisely the neglect of the non - adiabatic term that allows us to reduce the given problem to two independent Schrödiger equations - electronic and nuclear. As shown in work, the electron equation does not depend on the mass of the nucleus, and therefore the energy eigenvalue is the same for different isotopes [46]. This conclusion, as well as the large of the isotopic shift energy, makes it necessary to search for new mechanism to describe the neutron - electron interaction, including subatomic physics [1,5].

The uniqueness of LiH_xD_{1-x} crystals, which made it possible to measure the energy of the zero - phonon emission line of free excitons in low - temperature luminescence spectra for different deuterium concentration opens up the possibility of quantitatively tracking the change in the strong interaction between a proton and a neutron depending in distance between them. Modern NP describes the stable state of atomic nuclei due to the residual strong interaction of quarks and gluons inside nucleons in the nucleus (analogous to the van der Waals interaction in atomic physics). Let us repeat that the quark - quark interaction carried by massless gluons inside nucleons is long - range, whereas the nucleon - nucleon interaction described by the Yukawa potential is short – range [17]. This is an old mystery that still has no consistent explanation in theoretical physics [2,3]. The modern model of the atomic nucleus, according to Iwanenko and Heisenberg, consists of protons and neutrons, around which small - mass electrons revolve, the interaction of which with protons is described in a simple electrostatic model [5]. Therefore, the well-known coefficient - the binding energy of a proton with an electron (equals to 13.6 eV) in the case of a sold it turns into a variable value of interband transitions Eg, is contained in any book on atomic physics [47,48]. The neutron, the second particle in the nucleus of an atom, has little studied properties. A demonstration of this is the lack of knowledge about the neutron - electron binding energy (see, for example [49]). Since the LiH (without strong force in hydrogen nucleus) and LiD (with strong force in deuterium nucleus) crystals we used in our experiments differ by only one neutron, all other crystal - forming particle are indeed the same, and addition of a neutron to the hydrogen nucleus, according to Yukawa generates a strong interaction between the proton and neutron in the nucleus, which om the other hand, causes the observed isotopic shift of the zero - phonon emission line of free excitons in the low - temperature luminescence spectra of LiD crystals see Figure. 1. Considering that the value of E_g (the binding energy of a proton and an electron) is the same in LiH and LiD crystals, the increase in E_g in LiD is caused by the addition of a neutron to the hydrogen nucleus. In this case the difference between zero phonon emission lines in LiD and LiH crystals is equal to the neutron - electron binding energy of 0.103 eV. Similarly, in work it was shown that the neutron - electron binding energy in diamond is equal to 105 ± 3 meV, and for Ge and ZnO it is equal to 108 ± 5 meV and to 122 ± 10 meV, respectively [50]. Data for Ge and ZnO crystals are taken from review [37]. A good agreement is evident with the data of Breit (106.7 meV) obtained from the results of scattering of electrons (their length) more than half a century ago in the electrostatic model [5,34]. Naturally with an increase in the number of nucleons in the nucleus, it is necessary to take into account the field contribution, which was not done in our estimates [18]. Thus, spectroscopic measurements of the mass isotopic shift it possible for the first time to determine the neutron - electron binding energy. Using subatomic physics to interpret the results of measuring the strong interaction from the distance between the proton and neutron in the deuterium nucleus in LiD crystals allows us to estimate the energy of the boson responsible for the interaction of the neutron and electron and secondly to calculate the coupling constant of the strong interaction at different values of the binding energy. For an interaction radius equals to the Bohr radius $a_0 = 0.52917706 \cdot 10^{-10}$m, the Yukawa potential gives a boson mass value of = 3.7 keV^+).

*) Relativistic units (h = c = 1) were used to obtain this estimate.

This is very small energy value if we take into account that the binding energy of a proton and a neutron in deuterium nucleus is 2.224 MeV [51]. The found value of the neutron - electron bond energy, despite the smallness of its magnitude, nevertheless, as will be shown, determines a rather large of the strong interaction coupling constant.

Below, the dipole - dipole magnetic interaction model will be used to estimate the coupling constant of the strong interaction. We are already familiar with the dipole-dipole magnetic interaction arising from the hyperfine splitting in the Hydrogen atom (for an adequate, to our purpose, study see [49]).

The ground state wave function for the electron in the Hydrogen atom, including the spin part, is

$$\psi_0 = (\pi a_0^3)^{-1/2} e^{-r/a_0} |s>, \qquad (2)$$

a_0 being the Bohr radius. We also need the energy of a magnetic dipole $\vec{m}_1$ in a magnetic field $\vec{B}$ produced by another dipole ($\vec{m}_2$) given by

$$H = -\vec{m}.\vec{B}.$$

$$H = -\frac{1}{4\pi}\frac{1}{r^3}[3(\vec{m}_1\hat{r})(\vec{m}_2\hat{r}) - \vec{m}_1.\vec{m}_2] - \frac{2}{3}(\vec{m}_1.\vec{m}_2)\delta^3(\vec{r}). \quad (3)$$

As is well known, for s states with spherical symmetry the first term vanishes and only the second term involving a delta

function contributes. This is essential as the wave function (1) has a finite value for $r = 0$ so that the energy comes out from a contact-interaction (see, for example [3]). The magnetic dipole-dipole interaction can thus be treated as a perturbation. In first order perturbation theory:

$$E' = \int \psi_0^* H \psi_0 dV. \tag{4}$$

As mentioned, only the second term contributes giving:

$$E' = -\frac{2}{3} < \vec{m}_1 . \vec{m}_2 > |\psi_0(0)|^2 = -\frac{2}{3} \frac{1}{\pi a_0^3} < \vec{m}_1 . \vec{m}_2 >. \tag{5}$$

For the electron-proton we have two configurations according to the spin of both particles:

$$\vec{m}_1 = \gamma_p \vec{S}_p, \vec{m}_2 = -\gamma_e \vec{S}_e.$$

(γ: gyromagnetic ratio. $\gamma = (e/2m)g$, the g-factor being 2.0023 for the electron and 5.5857 for the proton).

According to equation (5), we obtain for the triple and singlet states in Hydrogen, the energies

$$E_t' = \frac{1}{3} \frac{e^2}{a_0^3 m_e M_p} g_p = 1.468510^{-6} eV$$

and

$$E_s' = -\frac{e^2}{a_0^3 m_e M_p} g_p = -4.4054 \cdot 10^{-6} \text{ eV},$$

with a gap ΔE‘= 5. 87410^{-6}, coincident with the hydrogen hyperfine splitting experimental result.

Similar calculations can be easily carried out for Deuterium (spin 1 and gyromagnetic ratio g_d= 1. 71 [43]) with the results

$$E_{3/2}' = 4.498010^{-7} eV$$

$$E_{1/2}' = -8.996010^{-7} eV$$

$$\Delta E_d' = E_{3/2}' - E_{1/2}' = 1.349410^{-6} eV.$$

Turning now to the Isotopic shift issue, from the above values, we have four alternatives depending on the relative spins, however, as the lowest energy for both LiH and LiD is the corresponding to singlet states, we shall choose:

$$\Delta E = (E_s')_H - (E_{1/2}')_D = -3.505810^{-6} eV, \tag{6}$$

far from the experimental 0.103 eV. Next, we shall assume that the experimental isotopic shift of 0.103 eV is the result of the onset of a residual strong interaction when the neutron is added, accordingly we do not modify $(E'_s)_H$ but modify $(E'_{1/2})_D$ in the following way: In Hydrogen the absolute value of the charge is the same so that in electric or magnetic interactions the coupling constant is $\alpha = e^2$. However, as the neutron do not have electric charge, in the dipole magnetic interaction the effective coupling constant can be defined through the transformation

$$\alpha = e^2 \longrightarrow (\alpha_s)_{eff} = e.e_s. \tag{7}$$

The Bohr radius is thus modified:

$$a_s' = \frac{1}{e.e_s} \frac{1}{m_e}.$$

From(4), it is easy to obtain (see, also [6])

$$(E_{1/2}')_D = -\frac{4}{3} g_d \frac{(\alpha_s')^4 m_e^2}{M_d}. \tag{8}$$

Inserting in (8) the 0.103 experimental value for ΔE and solving for α‘ , we obtain:

$$\alpha_s' = 0.1342,$$

and a *strong charge*

$$e_s = \frac{0.1342}{0.08542} = 1.5710$$

leading to a strong coupling constant $e^2_s = \alpha s$ = 2. 4680. Quite large in comparison with the normal fine structure constant. In high energy physics this value is usually equal to $\alpha_s(M_Z) = 0.1198 \pm 0/002$ [52]. Note that regardless of the nature of the magnetic interaction (electromagnetic or color), the value of the strong interaction coupling constant is more than 20 times greater than the similar value of a distance of femtometers in NP and EPP. Using formula (8), we calculated the value α_s as a function of the neutron - electron binding energy. The calculation results are presented in Figure.4.

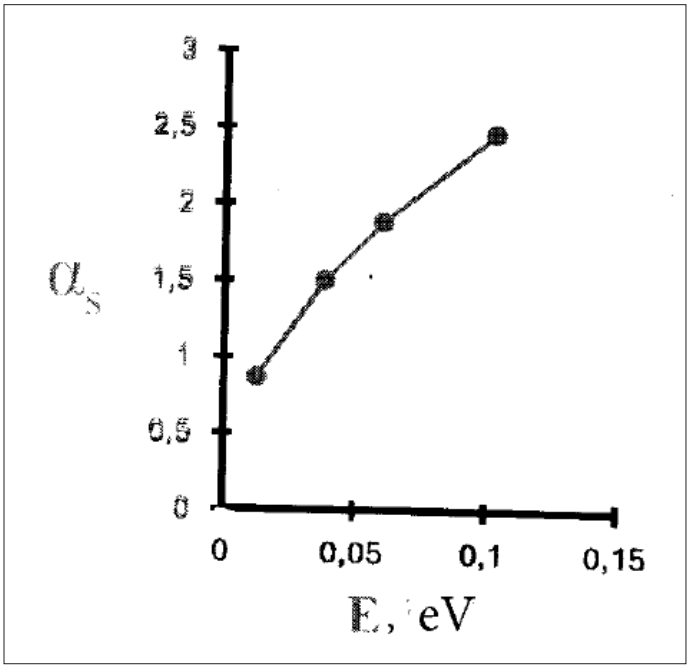

Figure 4: Dependence of the strong interaction coupling constant on the neutron - electron binding energy.

The observed nonlinear dependence coupling constant may be caused by the

manifestation of a new unknown force of electromagnetic or color origin in the mass isotope effect. Let us also note that more than forty years ago, hints on the manifestation of a new force or higher terms of expansion of electromagnetic origin were expected by the author of the world - famous monograph on the isotopic shift in atomic spectra [18]. It should be added here

that the authors of the already cited works [27-33] are also busy searching for deviations from the King linearity in isotopic shift of heavy chemical elements in the hope that in this way they will be able to find either a new force or a new boson that carries out the neutron - electron interaction [1].

B) Diamond and Graphene

Another very interesting example is carbon. Carbon atom is built from 6 protons, A neutrons and 6 electrons, where A = 6 or 7, yield the stable isotopes ^{12}C and ^{13}C, respectively, and A = 8 characterizes the radioactive isotope ^{14}C [53]. The isotope ^{12}C, with nuclear spin I = 0, is the most common one in nature with 99% of all carbon atoms, whereas only = 1% are ^{13}C with nuclear spin I = 1/2. There only traces of ^{14}C (10^{-12} of all carbon atoms) which transforms into nitrogen ^{14}N by β - decays [54]. Although ^{14}C only occurs rarely, it is important isotope used for historical dating (see, e.g. [55]). Carbon, one of the most elements in nature, still gives a lot surprises. It is found in many different forms - allotropes (Figure 5) - from zero-dimensional fullerene, one dimensional carbon nanotubes, two-dimensional graphene and graphite, to three-dimensional diamond - and the properties of the various carbon allotropes can vary widely [21,53]. Fullerenes are essentially hollow carbon shells of various sizes. the most well - known of these is a 60 - carbon unit called Buckminster fullerene or C_{60} (the more details see below). For instance, diamond is the hardest material, while graphite is one of the softest; diamond is transparent to the visible part of spectrum, while graphite is opaque; diamond is an electrical insulator, while graphite and graphene are a conductor. Very important is that all these different properties originate from the same carbon atoms, simply with different arrangements of the atomic structure. Below we describe the new phenomena of the carbon - isotope effect in diamond. Crystals ^{12}C and ^{13}C diamond differ only one neutron.

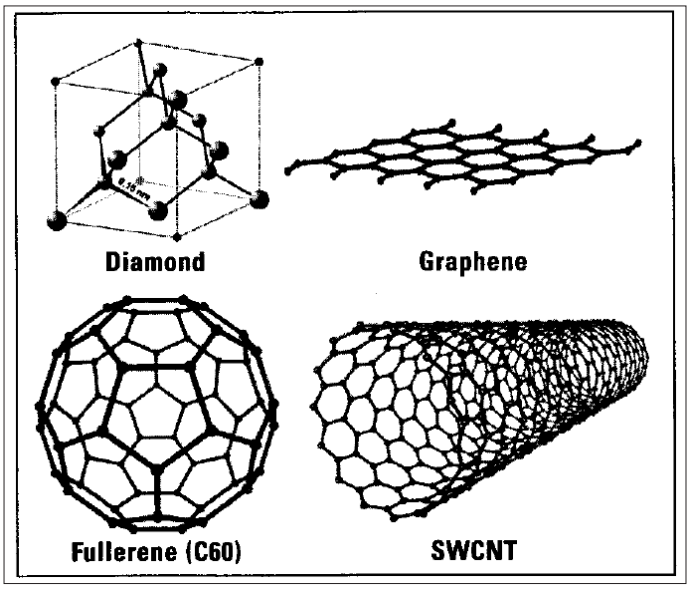

Figure 5: Structure of some representative carbon allotropes [diamond, graphene, fullerene (C60) and SWCNT].

In the atomic ground state of carbon, the 6 electrons are in the configuration $1s^2 2s^2 2p^2$, i.e. 2 electrons fill the inner shell 1s, which is close to the nucleus and which is irrelevant for chemical reactions, whereas 4 electrons occupy the outer shell of 2s and 2p orbitals. Because the 2p orbitals ($2p_x$, $2p_y$ and $2p_z$) are roughly 4 eV higher than the 2s orbital, it is energetically favorable to put 2 electrons in the 2s orbital and only 2 of them in the 2-p orbital (see, e.g. [1,57]). It turns out, however, that in the presence of other atoms, such as e.g. H, O, or other C atoms, it is favorable to excite one electron from the 2s to the third 2p orbital, in order to form covalent bonds with the other atoms. The gain in energy from the covalent bond is indeed larger than the 4-eV invested in the electronic excitation. In the excitation state, we therefore have four equivalent quantum - mechanical states: $|2s\rangle$, $|2p_x\rangle$, $|2p_y\rangle$ and $|2p_z\rangle$. a quantum - mechanical superposition of the state $|2s\rangle$ and $n|2p_j\rangle$ states is called spn hybridization, which play an essential role in carbon bonds [57].

In the case of a superposition of the 2s and two 2p orbitals, which we may choose to be the $|2p_x\rangle$ and the $|2p_y\rangle$ states, one obtains the planar sp^2 hybridization. The three quantum - mechanical states are given by

$$|sp_1^2\rangle = \frac{1}{\sqrt{3}} |2s\rangle - \sqrt{\frac{2}{3}} |2p_y\rangle,$$

$$|sp_2^2\rangle = \frac{1}{\sqrt{3}} |2s\rangle + \sqrt{\frac{2}{3}} \left(\frac{\sqrt{3}}{2} |2p_x\rangle + \frac{1}{2} |2p_y\rangle\right), \quad (9)$$

$$|sp_3^2\rangle = -\frac{1}{\sqrt{3}} |2s\rangle + \sqrt{\frac{2}{3}} \left(-\frac{\sqrt{3}}{2} |2p_x\rangle + \frac{1}{2} |2p_y\rangle\right).$$

These orbitals are oriented in the xy - plane and have nutual 1200 angles (Figure. 6a). The remaining unhybrized $2p_z$ orbitalis perpendicular to the plane A prominent chemical example for such hybridization is the benzene molecule [57]. This molecule consists of a hexagon with carbon atoms at the corner linked by σ bonds (Figure 6b). Each carbon atom has, furthermore, a covalent bond with one of the hydrogen atoms which stick out from the hexagon in a star like manner. In addition to the 6 bonds, the remaining $2p_z$ orbitals form 3л bonds, and the resulting double bonds alternate

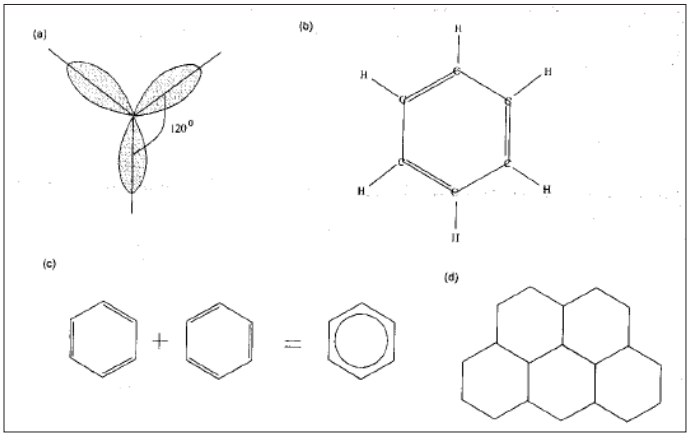

Figure 6: (a) Schematic view of the sp^2 hybridization. The orbitals form angles of 120^0. (b) Benzene molecule - C_6H_6. The 6 carbon atomsare situated at the corners of a hexagon and form covalent bonds with the H atoms. In addition to the 6 covalent σ bonds between C atoms, there are three $л$ bonds indicated by the doubled line. (c) The quantum - mechanical ground state of the benzene ring is a superposition of the configurations which differ by the position of the $л$ bonds. The $л$ electrons are, the

delocalized over the ring. (d) Graphene may be viewed as a tiling of benzene hexagons, where the H atoms are replaced by C atoms of neighbouring hexagons and where the л electrons are delocalized over the whole structure.

with single σ bonds around hexagon. Because a double bond is stronger than a single σ bond, one may expect that the hexagon is not perfect. A double bond (C = C) yields a carbon - carbon distance of 0.135 nm, whereas it is 0.147 nm for a single σbond (C - C). However, the measured carbon - carbon distance in benzene is 0.142 nm for all bonds, which is roughly the average length of a single and a double bond. The ground state a quantum - mechanical superposition of the two possible configurations for the double bonds shown schematically in Figure 6[c]. These chemical considerations indicate the way towards carbon - based condensed matter physics - any graphitic compound has been a sheet of graphene as its basic constituent. Such a graphene sheet may be viewed simply as a tiling of benzene hexagons, where one has replaced the hydrogen by carbon atoms to form a neighboring carbon hexagon (see Figure 6[d]). However, graphene has remained the basic constituent of graphitic systems during a long time only on the theoretical level. From experimental point of view, graphene is the youngest allotrope and accessible to physics measurements only since 2004. Graphite may be viewed as a stacking sheet (Figure.6[c]) that stick together due to the van der Waals interaction, which is much weaker than in plane covalent bonds [56].

If one superimposes the 2s and all three 2p orbitals, one obtains the sp3 hybridization, which consist of four club - like orbitals that mark a tetrahedron. The orbitals forma angles of 109.5^0 degrees (Figure 7[a]). A chemical example for this hybridization is methane (CH_4), where the four hybridized orbitals are used to form covalent bonds with the 1s hydrogenatoms. In condensed matter physics, the $2p^3$ hybridization is at the origin of the formation of diamonds, when liquid carbon condenses under high pressure. The diamond lattice consists of two interpenetrating face - center - cubic (fcc) lattice as, with a lattice spacing of 0.357 nm as shown in Figure 7[b].

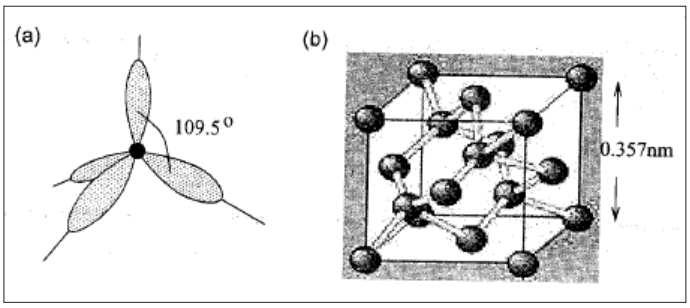

Figure 7: (a) sp^3 hybridization with 109.5^0 angle between the four orbitals. (b) Crystal structure of diamond.

Although they consist of the same atomic ingredient, namely carbon, the 3D graphite and diamond crystals are physically extremely different. Graphite, as described above is a very soft material due to its layered structure, whereas diamond is one of the hardest natural materials because all bonds are covalent σ bonds [1]. The fact that all 4 valence electrons in the outer atomic shell are used in the formation of the σ bonds is also the reason for diamond being an insulator with a large band gap of 5.47 eV (see above). In contrast to insulating diamond, the electrons in the weaker л bonds in graphite are delocalized and thus, yield good electronic conduction properties. The absorption spectrum demonstrating an indirect electronic transition in diamond is presented in Figure 8.

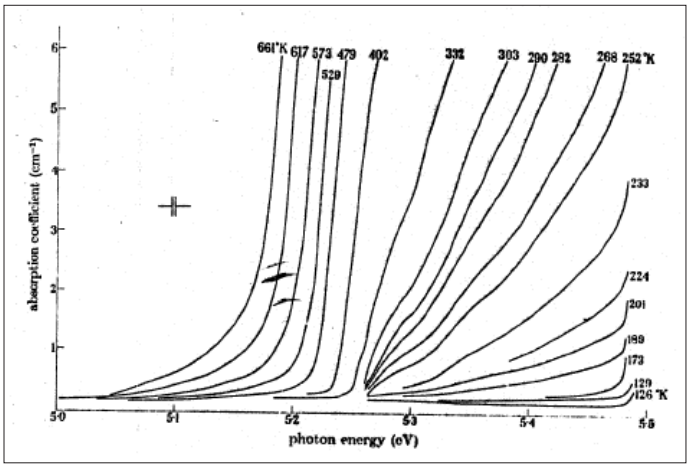

Figure 8: Absorption edge spectrum of diamond at various temperature [58].

The indirect transition diagram is shown in Figure. 9. In diamond, we have seen (Figure 2.5 in [62]) that excitation across the minimum separation of filled and empty states demands a large change in wave vector, and such a transition cannot be initiated by a photon unless it has access to a source of crystal momentum. We should repeat that it is the phonons that provide the required momentum (see, also Figure.9).

We write the conservation laws in the form

$$E_f - E_i = h\nu + \hbar\omega_f, \qquad \vec{k_f} - \vec{k_i} = 0 + \vec{q}, \qquad (10)$$

here q and ω_f apply to the phonon involved in the transition. Now $E_f - E_i = E_g$ and it is clear that the inclusion of phonons produces an absorption edge at a somewhat lower energy, namely $E_g - \hbar\omega_f$ huf. These indirect or phonon - assisted transitions produce only weak absorption compared with that associated with direct transitions (see, e.g. [57]).

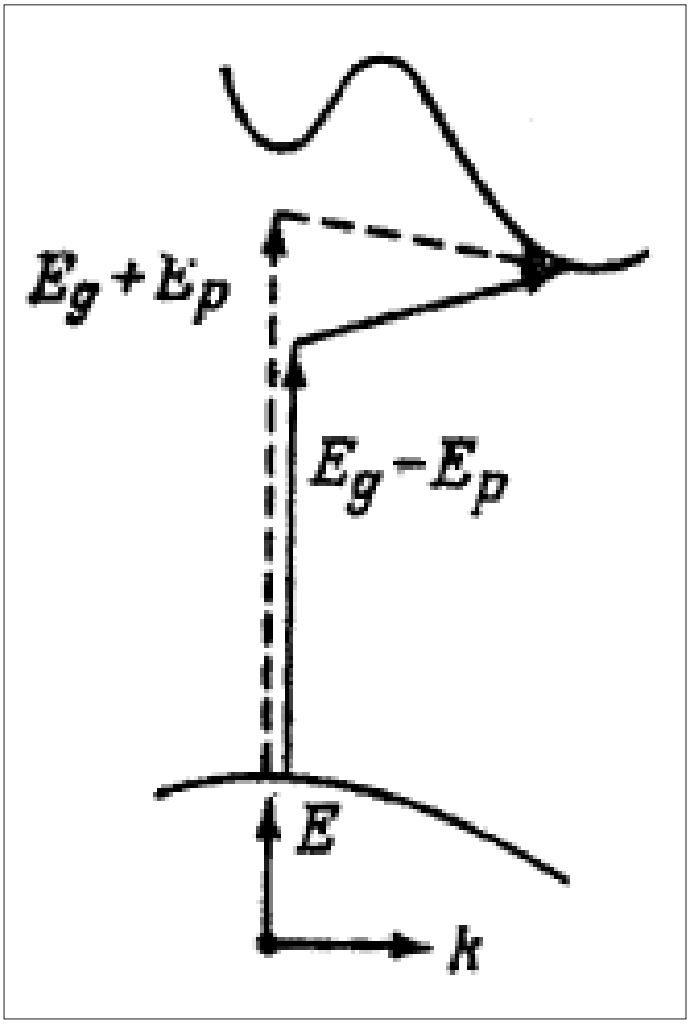

Figure 9: Schematic of two - step transition in the case of the indirect band gap of material, where E_p is the phonon energy and E_g is the energy of interbond transition.

Due to the indirect gap of E_g = 5.47 ± 0.005 eV (295 K), at K = 0.76 X, diamond has intrinsic phonon - assisted free exciton luminescence lines (see, e.g. [37]). The change of the indirect gap of diamond between pure ^{12}C and ^{13}C crystals has been determined by Collins et al. [59]. The luminescence spectra of the natural (^{12}C) and synthetic (^{13}C) diamond at electron excitation were investigated by Collins et al. [59] (Figure 10), Ruf et al., Watanabe et al. [60,61]. Figure 10 compares the free exciton luminescence for a natural diamond with that for a synthetic diamond.

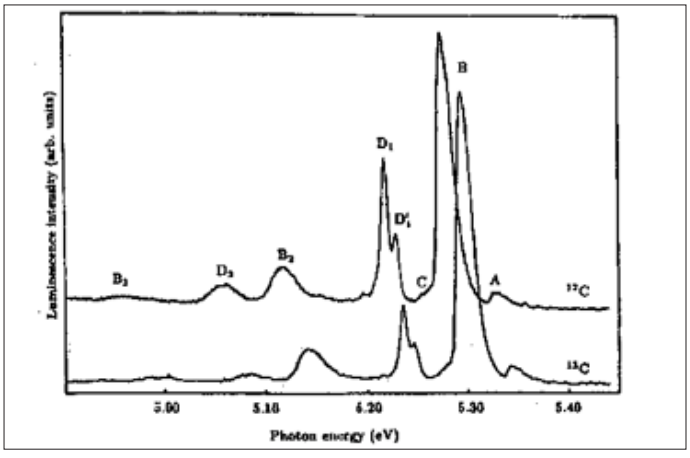

Figure 10: Spectra measured at 77K phonon - assisted free cathodoluminescence feature (A, B and C) and the phonon assisted bound - exciton feature (D) from natural semiconducting ^{12}C diamond and a ^{13}C synthetic diamond (after [59]).

The peaks labeled A, B and C are due, respectively, to the recombination of a free exciton with the emission of transverse - acoustic, transverse - optic and longitudinal - optic phonons having wavevector ± k_{min} and quanta in ^{12}C [37,62].

$$\hbar\omega_{TA} = 87 \pm 2;\ \hbar\omega_{TO} = 141 \pm 2;\ \hbar\omega_{LO} = 163 \pm 1 \text{ meV}. \quad (11)$$

Features B_2 and B_3 are further free exciton processes involving the above TO phonon with one and two zone - center optic phonons respectively. As we can see from Figure 12 the isotope shift of the free exciton luminescence spectrum of 13C diamond is equal 16.5 ± 2.5 meV [37]. The more detailed and quantitative investigation of $E_g \sim f(x)$, where x is the isotope concentration was done by Ruf et all. (Figure. 11) and Watanabe et all. (Figure. 12) where five samples of diamond with different concentrations x were studied [60,61].

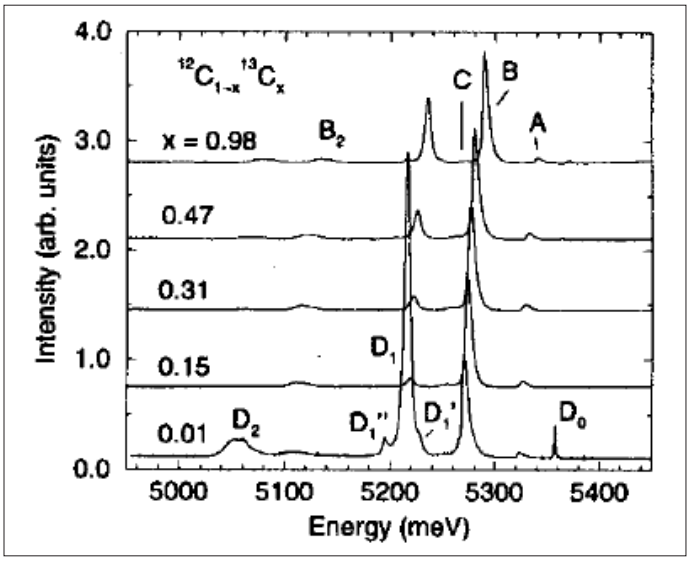

Figure 11: Cathodoluminescence spectra of isotopically modified diamond at 36K. Intrinsic phonon - assisted recombination peaks are labeled in the top spectrum, those from boron - bound excitons in that at the bottom. The spectra are normalized to the intensity of the B peak and vertically offset for clarity (after [60]).

Watanabe et al. have concluded that the maximum change of the band gap due to substitution of ^{12}C by ^{13}C is ΔE_g = 15.4 meV. The dependence of the change exciton energy on the isotopic concentration in a diamond is depicted on the Figure 13.

This value (15.4 meV) is in good agreement with the estimate of 16.5 ± 2.5 meV by Collins et all. using a zero - point renormalization obtained from a fit of the experimental temperature dependence of the band gap [59]. We should stress that the isotope shift in $^{12}C^{13}C_{1-x}$ diamond crystals approximately 15 meV per one neutron and on seven neutrons we get 15 • 7 = 105 mev. This value is very close to the observed one (0.103 meV) in LiH_xLiD_{1-x} crystals. As will be shown below this value is the maximum value of the neutron - electron binding energy.

It is clear that the lattice - dynamic properties of a crystal are directly affected by the atomic mass. To a first approximation, phonon behave like harmonic oscillators with frequencies [59]

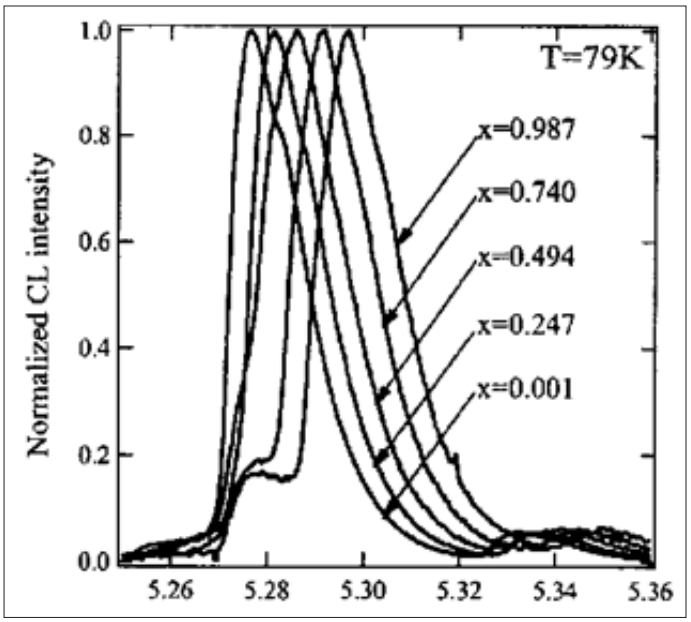

Figure 12: luminescence spectra of free excitons in homoepitaxial diamond films grown from mixture of methane in hydrogen by means of a microwave plasma - assisted CVD. The spectra illustrate the effect of isotope composition $12C^{13}_{1-x}C_x$ mixed in the CVD gas phase. All spectra ate normalized to the same height (after [61]).

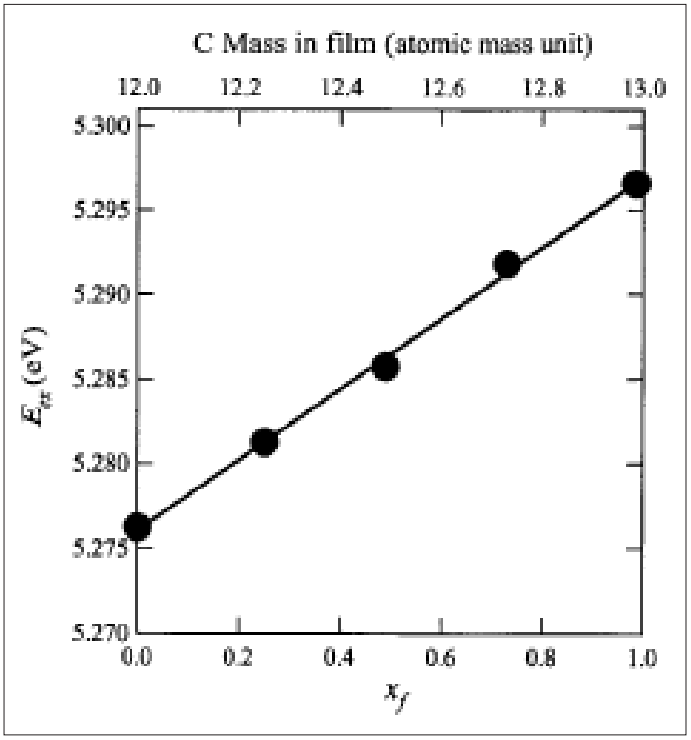

Figure 13: Excitonic band - gap energy E_{exc} obtained for the CL peak energes in Figure. 14 as a function of the ^{13}C concentration of the films (x_f). The solid line is a linear regression fit of the data (after [61]).

$$\omega \propto m^{-1/2}. \qquad (12)$$

Crystals containing various isotopes are usually described within virtual crystal approximation (VCA) [37] where m in Eq. (12) is replaced by the average atomic mass

$$\overline{m} = \sum_i c_i m_i. \qquad (13)$$

It is obtained from the sum over the isotope's masses mi and concentration ci. In spite of VCA simplicity, the model describes the general feature of the lattice dynamics of mixed alkali - halide crystal sufficiently well (for details see [59,62]). Isotopes are ideal for lattice - dynamitic investigations of crystals. One can make use of the unique isotopic properties by varying the isotopic composition. Isotope substitution helps to disentangle the individual contributions of anharmonic and disorder - induced effects and to clarity the origin of phonon broadening mechanisms. Due to the fact that substitution of the isotopic mass in semiconducting crystals a small variation of E_g, perturbation theory is applicable (excluding LiH crystals [62,38]).

Raman spectroscopy is a powerful means to gain experimental access to phonons and their interaction and scattering mechanisms. All studies presented in this paragraph are restricted to stable, i.e. non - radioactive isotopes. About 300 stable and 1000 radioactive isotopes are known today. Some elements are isotopically pure (for example, Co), while others may contain numerous isotopic modifications (for example, Sn has 10 stable isotopes with atomic masses ranging from 112 to 124, while Xe has 23 isotopes, 9 of which are stable (see, Table 1 in [62]).

In this part, the modern understanding of first - order Raman slight scattering spectra in isotopically mixed elementary and compound (CuCl, GaN, GaAs, GaP) semiconductors having a zinc blende structure is described. It is well - known that materials having a diamond structure (C, Si Ge, α - Sn) are characterized by the triply degenerate phonon states in the F - point of the Brillouin zone (k = 0) (see, e.g. [55]). Isotope effect in light scattering spectra in Ge crystals was first investigated by Agekyan et al. [63]. A more detailed study of Raman light scattering spectra in isotopically mixed Ge crystals has been performed by Cardona and coworkers [62].

The cubic modifications of crystalline carbon, diamond, is characterized by a tetrahedral coordination underlying its structure dictated by sp^3 bonding (see Figure 7) between the nearest neighbor atoms. Diamond has two atoms per primitive (Bravais) cell. The strong covalent bonding and the light mass of the constituent atoms result in a large frequency for zone center, Raman active, triply degenerate F_2 mode [64]. Its crystalline perfection and transparency make diamond ideally suited for inelastic light scattering [37]. First Raman study of the dependence the frequencies of phonons on the isotopic composition was conducted on diamond by Chrenko in 1988 [66]. Several publications on diamond by other groups followed later [64-66]. Most clear results were obtained by Hanzawa et al. (see Figure 14) [65].

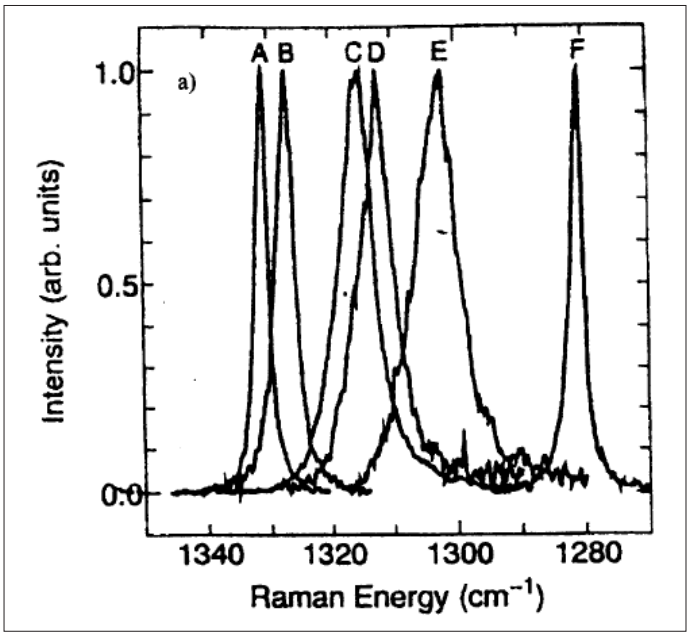

Figure 14: First - order Raman scattering in isotopically mixed diamond crystals $^{12}C^{13}C_{1-x}$. The peaks A, B, C, D, E and F correspond to x = 0.989; 0.90; 0.60; 0.50; 0.30 and 0.001(after [65]).

First - order Raman light scattering spectrum in diamond crystals also includes one line with maximum $_{uLTO}$(F) = 1332.5 cm^{-1} [65]. In Figure 14 the first - order scattering spectrum in diamond crystals with different isotope concentrations is shown [65]. As was shown in, the maximum and width of the first - order scattering line in isotopically - mixed diamond crystals are nonlinearly dependent on the concentration of isotopes x [62]. The maximum shift of this line is 52.3 cm^{-1}, corresponding to the two limiting values of x = 0 and x = 1. The effect of the isotopic ^{12}C to ^{13}C ratio on the first - and second - order Raman scattering of light in the diamond has been investigated in [69]. As ^{13}C content is increased from the natural ratio ($^{12}C/^{13}C$ = (1 - x)/x, where x = 0.011 to the almost pure ^{13}C (x = 0.987) the whole spectrum has shifted towards longer wavelength (Figure 15) in good agreement with the expected M–0.5 frequency dependence on the reduced mass M. For an approximately equal mix of the two isotopes, the authors reported that the feature seen in the above two - phonon spectra were either broadened or unresolved.

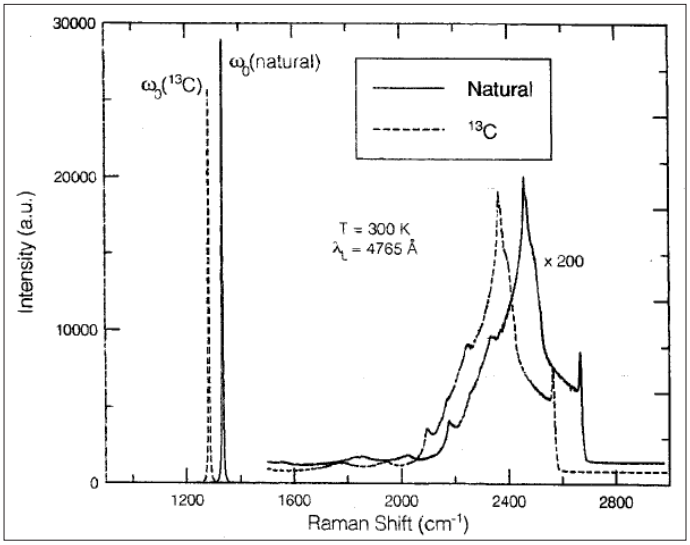

Figure 15: The Raman spectra of natural and a 13C diamond. The spectra show the dominant first - order Raman - active F_{2g} line and the significantly weaker quasi - continuous multiphonon features (after [69]).

The measured dependence on average mass mainly reflects the isotope effect on the harmonic frequency (Eq. (12)) which is, however, modified by anharmonic and disorder - induced contributions [37,62]. Isotope renormalization frequencies of phonons of other semiconducting crystals (GaP, GaAs, α - Sn, ZnS, ZnO, CuCl, CuBr) was published in the next reviews [38]. We should highlight that addition one next neutron in nuclei is called the change in more or less of energy of elementary excitations in solids.

The science of the nuclear, atoms, simple molecules and the science of matter from microstructure to larger scales are well established. A remaining, extremely important, size related challenge is at the atomic scale, roughly the dimensional scale between 1 and 10 molecular sizes, where the fundamental properties of materials are determined and can be engineered (see also [55]. This field of science – isotopetronics - is a broad and interdisciplinary field of emerging research and development [37,62]. Isotopetronics is connected to materials, structures and systems which components, as in nanoscience, exhibit novel and significantly modified physical properties due to their small sizes [55]. The method of the isotope renormalization of the energy of elementary excitations in bulk solid and low - dimensional structures very often used in the last five decades and well documented in the scientific literature (see [37,62] and references quoted therein). In this paper, current understanding of the band - gap opening in graphene is discussed along with associated experimental and theoretical investigations.

As was shown above, carbon, one of the second basic elements in nature after silicon, still gives a lot surprises. It is found in many different forms - allotropes - from zero-dimensional fullerene, one dimensional carbon nanotubes, two-dimensional graphene and graphite, to three-dimensional diamond (Figure 7) - and the properties of the various carbon allotropes can vary widely [21]. For instance, diamond is the hardest material, while graphite is one of the softest: diamond is transparent to the visible part of spectrum, while graphite is opaque; diamond is an electrical insulator, while graphite is a conductor. Very important is that all these different properties originate from the same carbon atoms, simply with different arrangements of the atomic structure.

In two-dimensional graphene, carbon atoms are periodically arranged in an infinite honeycomb lattice Figure16a. Such an atomic structure is defined by two types of bonds within the sp^2 hybridization. From the four valence orbitals of the carbon atom (the 2s, $2p_x$, $2p_y$, and $2p_z$ orbitals, where z is the direction perpendicular to the sheet), the (s, p_x, p_y) orbitals combine to form the in plane σ (bonding or occupied) and σ* (antibonding or unoccupied) orbitals. Three σ –bonds join a C atom to its three neighbors. They are quite strong, leading to optical - phonon frequencies much higher than observed in diamond (see below). Such orbitals are even with respect to the planar symmetry. The σ bonds are strongly covalent bonds determining the energetic stability and the elastic properties of grapheme. The remaining

p_z orbital, pointing out of the graphene sheet is odd with respect to the planar symmetry and decoupled from the σ states. From the lateral interaction with neighboring p_z orbitals (called the ppл interaction), localized л (bonding) and л* (antibonding) orbitals are formed [71]. Graphite consists of a stack of many graphene layers. The unit cell in graphite can be primarily defined using two graphene layers translated from each other by a C-C distance (a_{c-c} =1.42 Å). The three-dimensional structure of graphite is maintained by the weak interlayer van der Waals interaction between л bonds of adjacent layers, which generate a weak but finite out-of-plane delocalization [57]. The bonding and antibonding σ bands are actually strongly separated in energy > 12 eV, at and therefore their contribution to electronic properties is commonly disregarded, while the bonding and antibonding л states lie in the vicinity of the Fermi level (Figure. 17). The two remaining л bands completely describe the low energy electronic excitations in both graphene and graphite (see [57] and references therein). The bonding л and antibonding л* orbitals produce valence and conduction bands (Figure. 17) which cross at the charge neutrality point (Fermi level of undoped graphene) at vertices of the hexagonal Brillouin zone. Carbon atoms in a graphene plane are located at the vertices of a hexagonal lattice.

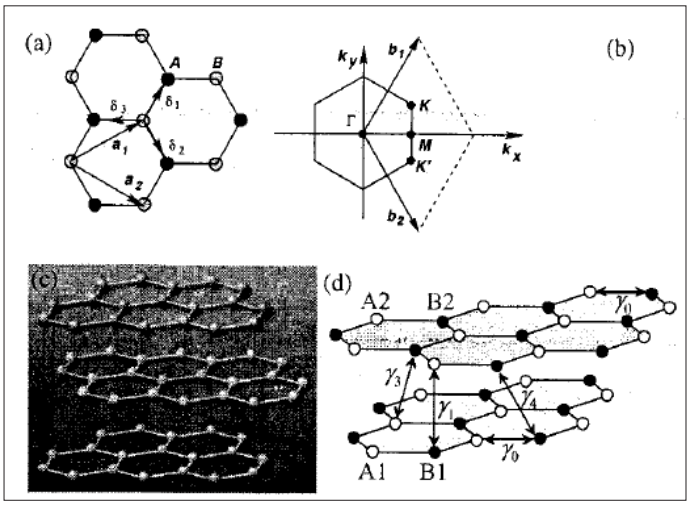

Figure 16: (a) Graphene honeycomb lattice showing the two triangular sublattices. (b) The graphene Brillouin zone in momentum space. (c) Lattice structure of graphite, graphene multilayer. (d) Lattice structure of bilayer graphene (explanation in text).

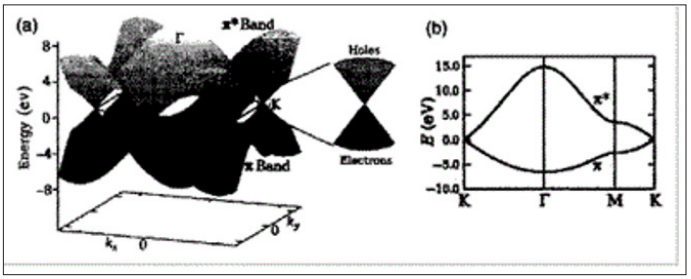

Figure 17: Energy dispersion of graphene obtained within the tight - binding approximation. a) Energy dispersion relation for graphene, drawn in the entire region of the Brillouin zone. Since in this approximation to ignore the coupling between the graphene sheets, the bands depend only on k_x and k_y. The л band is completely filled and meets the totally empty $л^+$ band at the K points. Near these points both bands linear dispersion as described in the literature. b) The dispersion along the high symmetry points FMK.

This graphene network can be regarded as a triangular Braves lattice with two atoms per unit cell (A and B). Each A- or B - type atom is surrounded by three atoms of the opposite type. In a simple neighbor model graphene is a semimetal with zero - overlap between valence and conduction bands. The energy dispersion of л electrons in graphene was first derived in 1947 by Wallace within the tight - binding approximation [71]. In this case, the wave function of graphene is a linear combination of Bloch function for sublattice A

$$\Phi_A = \frac{1}{\sqrt{N}} \sum_{\vec{R_A}} e^{i\vec{k}\vec{R_A}} \varphi(\vec{r} - \vec{R_A}), \qquad (14)$$

and equilibrium function Φ_B for the B sublatice. Here N is the number of unit cells, $\vec{R_A}$ are the position of the atom A and φ $(\vec{r} - \vec{R_A})$ is the 2pz orbital of the atom at $\vec{R_A}$. The sum runs over all unit cells, i.e. all possible lattice vectors. In the nearest neighbor approximation (every A site has three nearest B sites, and vice versa), the energy eigenvalues can be obtained in a closed form [56,57]

$$\varepsilon(k_x, k_y) = \pm \gamma_0 \left[1 + 4\cos\frac{\sqrt{3}k_x a}{2}\cos\frac{k_y a}{2} + 4\cos^2\frac{k_y a}{2}\right]^{1/2}, \qquad (15)$$

where γ0 is the transfer integral between the nearest neighbors. The energy dispersion of two - dimensional graphene according to this formula is plotted in Figure.2(a) as a function of the wave vector $\vec{k}$. The upper half of the curves are called the л* or the antibonding band while the lower one is л or the bonding band. The two bands degenerate at the two K points given by the reciprocal space vectors $\vec{K}$ = (2л/a)(1/3, 1/ 3) and $\vec{K}$ = (2л/a)(- 1/3, 1/ 3) points where the dispersion vanishes (see above).

Basically, graphene has redefined the limits of what a material can do: it boasts record thermal conductivity and the highest current density at room temperature ever measured (a million times that of copper!); it is the strongest material known (a hundred times stronger than steel!) yet is highly mechanically flexible; it is the least permeable material known (not even helium atoms can pass through it!); the best transparent conductive film; the thinnest material known; and the list goes on ...[56]. In the vicinity of K - points (as it can be seen from Figure. 17), the low - energy electron/ hole dispersion relation is proportional to momentum, rather than its square. This is analogous to the energy dispersion relation of massless relativistic electrons, so the electrons/holes of graphene are described as Dirac fermions having no mass. In a simple neighbor model graphene is a semimetal with zero - overlap between valence and conduction bands. In order to make graphene a real technology, a special issue must be solved: creating an energy gap at K - points in the Brillouin zone [57]. Different attempts have been made by researches, such as patterning graphene into nanoribbon, forming graphene quantum dots], making use of multilayer graphene sheets and applying an external electric field [72-76]. It was shown that the uniaxial strain can open a band - gap in a metallic carbon nanotube as well as carbon nanoribbon [73,74].

As it can be seen from Figure. 12 the band gap of ^{13}C has increased by 13.6 meV. Numerous examples of band gap increment at hard isotope substitution were collected in the papers [37,62]. The effect of the isotopic ^{12}C to ^{13}C ratio on the first and second - order Raman scattering of light in the diamond has been investigated in [61,69]. As the ^{13}C content is increased from the natural ratio ($^{12}C/\ ^{13}C = (1 - x) / x$, where x = 0.011), to the almost pure ^{13}C (x = 0.987), the whole spectrum has shifted towards longer wavelengths (see Figure. 16) in good agreement with the expected $M^{-0.5}$ frequency dependence on the reduced mass M. For an approximately equal mix of the two isotopes, the authors reported that the features seen in the above two - phonon spectra were either broadened or unreasonable. We should stress that the main line in the first - order Raman scattering spectrum of light at u 1332 cm^{-1} also shifts to the short-wavelength side on the 52.3cm^{-1} [37,62].

Elastic and inelastic light scattering are powerful tools for investigating graphene [77-83]. Raman spectroscopy allows monitoring of doping, defects, disorder, chemical and isotope modifications, as well as edges and uniaxial strain (see Figure. 20) [1].

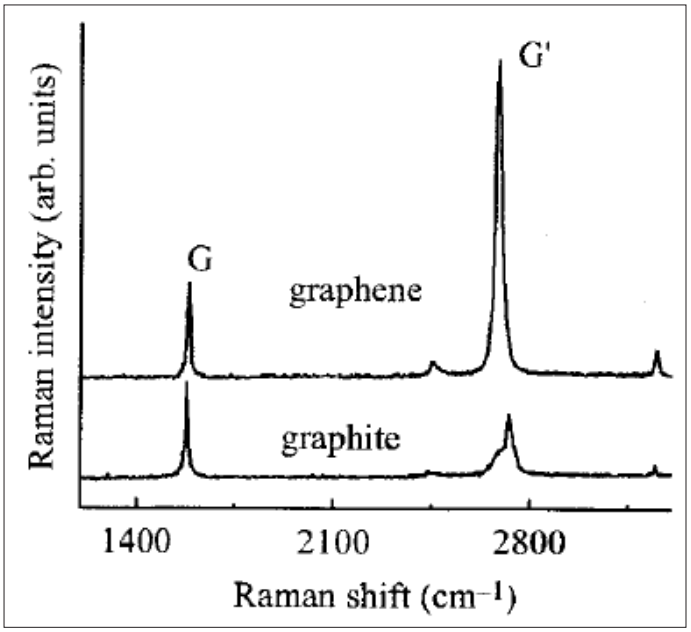

Figure 18: Comparison of the Raman spectra of graphene and graphite measured at room temperature and at the excitation at E_{laser} = 2.41 eV (514.5 nm).

All sp^2 - bonded carbons show common features in their Raman spectra, the so - called G and D peaks (see, Figure. 18), around 1580 and 1360 cm^{-1} (see, e.g. [56]). The G peak (see, also below Fig. 20) corresponds to the E2g phonon at the Brillouin zone center (F - point). The D peak is due to the breathing modes of six - atom rings and requires a defect for its activation. It comes from TO phonons around the Brillouin zone K point and it is activated by an intravalley scattering process. The 2D peak is the second order of the D peak. This is a single peak in monolayer graphene, whereas it splits into four bands in bilayer graphene, reflecting the evolution of the band structure [1,56]. The Raman spectrum of graphene also shows significantly less intensive defect - activated peaks such as the D' peak, which lies at ~ 1620 cm^{-1}. This is activated by an intravalley process i.e. connecting two points belonging to the same cone around K (see, Figure. 6 in [1]). The second order of the D' peak is called 2D' peak. Since 2D and 2D' peaks originate from a Raman scattering process where momentum conservation is obtained by the participation of two phonons with opposite wave vector (q and - q), they do not require the presence of defects. Thus, they are always visible in the Raman spectrum (see cited papers [19, 20, 23] and references therein).

Graphene is one unique material which shows properties not fond in other materials. One of these unique features of graphene is the influence of long-range strains on the electronic properties. The possibility of tuning the dynamics of carriers as well as phonons by appropriately designed strain patterns opens the way for novel applications of graphene, not possible with any other materials. At present time we have several reports, which have examined graphene properties under uniaxial deformation [1,56,84,85,86,87].

Strain can be very efficiently studied by Raman spectroscopy since this modifies the crystal phonon frequency, depending on the anharmonicity of the interatomic potentials of the atoms. Raman spectra of strained graphene show significant redshifts of 2D and G band (see Table 2) because of the elongated of the carbon - carbon bonds.

Table 2: Red shift of the G and 2D bands in the Raman spectra in graphene monolayers under uniaxial tensile

Ref.	Shift of G (G^+ and G^-) band cm^{-1}/%	Shift of 2D band cm^{-1}/%	E_g, meV
15	14.2	27.8	300
25	5.6; 12.5	21	
27	10.8; 31.7	64	
26			
theory			≃ 500

The authors of the paper have proposed that by applying uniaxial strain on graphene, tunable band - gap at K - point can be realized [86]. First principal calculations predicted a band - gap opening of = 300 meV for graphene under 1% uniaxial tensile strain (Figure. 21). Thus, the strained graphene provides an alternative way to experimentally tune the band - gap of graphene, which would be more efficient and more controllable than other methods (see, above) that are used to open band - gap in graphene.

The method of the isotope renormalization of the energy of elementary excitations in solid very often used in last five decades and well described in the scientific literature (see, for example reviews [37,38,62]). At now there is a large list of the paper devoted to investigation of the isotope - mixed graphene [1,56,82]. Chen at al. have reported the first experimental study of the isotope effect on the thermal properties of graphene [83]. The thermal conductivity K, of isotopically pure ^{12}C (0.01 of ^{13}C) graphene determined was higher than 4000 W/mK (approximately two times more than it in diamond) at the measured temperature T_m ~ 320K, and more than a factor of two

higher than the value of K in a graphene sheets composed of a 50% - 50% mixture of ^{12}C and ^{13}C [83, 56]. Raman spectroscopy transferred to the 285 nm SiO_2/Si wafer was performed under 532 nm laser excitation [83]. The G peak and 2D band positions in Raman spectra of graphene with 0.01%, 1.1%, 50% and 99.2% ^{13}C - isotope are presented in Figure. 20.

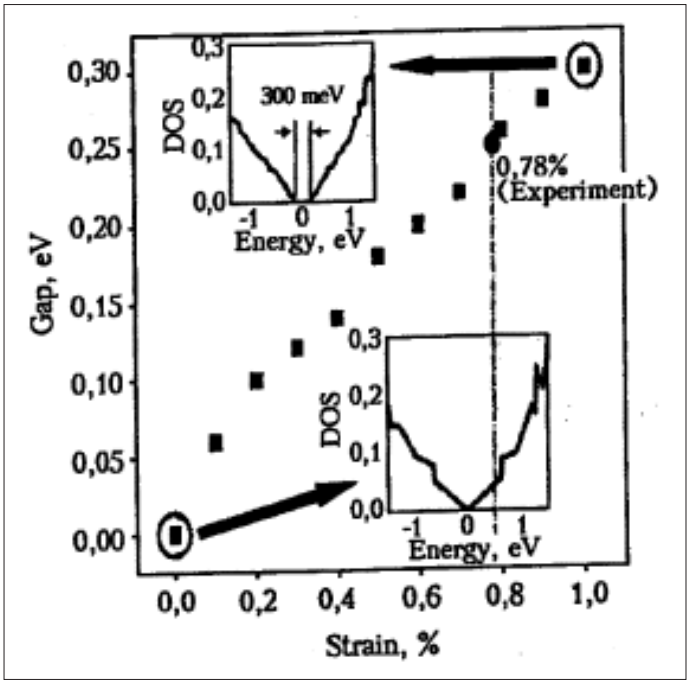

Figure 19: The band - gap of strained graphene with the increase of uniaxial tensile strain on graphene. The magnitude of gap is determined by the gap opening of density of states. The insets show the calculated density of states of unstrained and 1% tensile strained graphene. The dash line and solid dot indicate the calculated bandgap of graphene under the highest strain (0.78 %) [86].

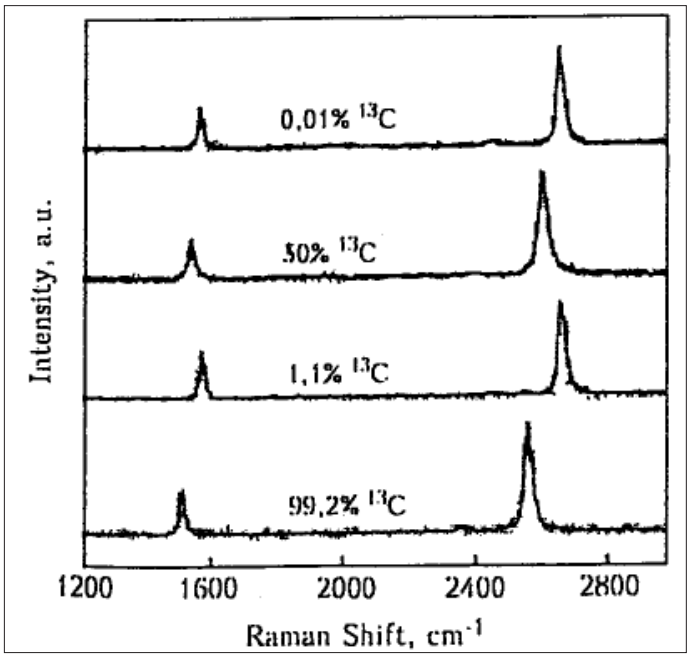

Figure 20: Raman spectra of graphene with different isotope concentration at room temperature [83].

Isotope shift of the G and 2D bands in the Raman spectra depicted on the Figure.20 [84].

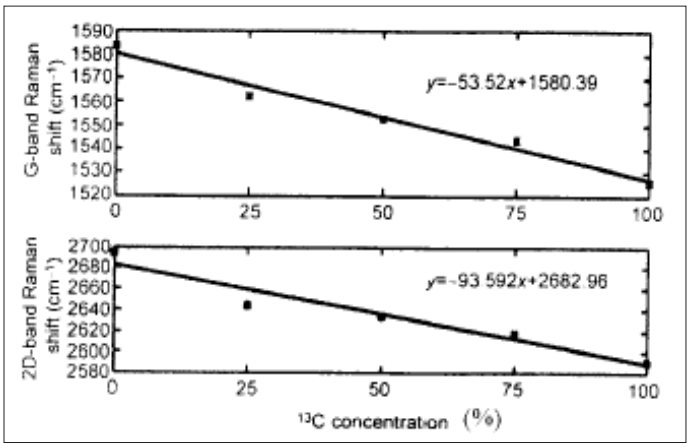

Figure 21: Peak position of G and 2D bands in Raman spectra as a function of the concentration of ^{13}C [88].

As in the case of isotope - mixed diamond the Brillouin - zone - center optical - phonon frequency u varies with the atomic mass M as $u \sim M^{-1/2}$ making the Raman shift for ^{13}C approximately $(12/13)^{-1/2}$ times smaller than that for ^{12}C [37,56,62]. The experimental difference between the lowest 99.2% ^{13}C and the highest 0.01% ^{13}C peak is ~ 64 cm^{-1} which is according in agreement with the theory, and attests for the high quality of isotopically modified graphene [62]. By the way we should indicate that in the Raman spectra in diamond (with sp^3 - bond) analogous shift of first - order line in Raman spectrum is equal 52.3 cm^{-1}, which is consistent with the isotope mass ratio [56]. Substituting a light isotope (^{12}C, H) with a heavy one increases the interbond transition energy in the case $^{12}C_x{}^{13}C_{1-x}$ on 14.7 meV and LiH_xD_{1-x} on 103 meV [38]. Taking into account a softer bond (sp^2 - bond instead sp^3 - bond in diamond) isotope - induced band - gap opening in graphene of some hundreds meV (up to E_g of Si) was predicted in paper (see, the more details below) [89].

Graphene has a two lattice parameters d and a [85]. When replacing the light ^{12}C isotope with the heavy ^{13}C isotope, a change in the parameters of the graphene hexagon is observed. The lattice constant d = 2.46E increases by 5%, while the magnitude an increase from 1.42Å to 1.5441 Å [85,94]. As it can easily see $\Delta a/a = 8\%$. Since a hexagon of graphene transforms into rectangular (Figure. 22) when stress is applied the average change in tension (compression) of graphene is 4% at the isotopic effect [93].

Using the results of the work of the authors we come to the conclusion that the isotopic effect causes an opening band gap in graphene up to a value equal to 1.2 eV till 2.4 eV [86]. This value is close to E_g value of silicon [62]. Thus, the introduction of an additional neutron into the carbon nucleus (^{13}C) increases the strong interaction according Yukawa the influence of which on the electron (lepton) in graphene stimulates the opening of the band gap [17]. The resulting E_g in ^{13}C graphene is quite close to value E_g = 3.4 – 3.7 eV hydrocarbon as well as fluographene [90,92].

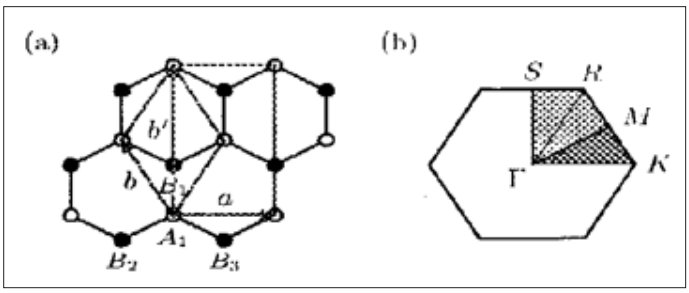

Figure 22: a) Graphene honeycomb lattice. It is formed from a triangular Bravais lattice with a two - atom basis consisting of A_1 and B_1, under uniaxial strain the Bravais lattice becomes centered rectangular. b) First Brillouin zone (see above text) [93].

With the opening E_g of massless fermions (leptons = electrons) acquire mass, estimates of different ways of opening E_g in graphene give the following equality: $E_g = 2m$, [95]. When E_g = 1.2 eV leptons acquire a mass equal 0.6 eV - the value is not large, but finite. One of the mechanisms of acquire mass in elementary particle physics is considered early [96]. This paper predicts that both quarks and gluons acquire running mass distribution in QCD, which are large at infrared momenta. Roberts shows that gluons are cannibals: they are parcel species whose members become massive by eating each other [97].

Conclusion

Man - made activation of a strong nuclear activation by adding one (two, etc.) neutron to an atomic nucleus leads to direct observation of the macroscopic properties of a strong nuclear interaction. The observation of an isotopic shift (0.103 eV) of the zero - phonon emission line in the low - temperature luminescence spectra of LiH (without strong interaction in the hydrogen nucleus) and LiD (with strong interaction in the deuterium nucleus) was first and direct evidence of the long - range interaction of the Yukawa potential. The macroscopic properties of strong interaction in crystals given in the review open up new possibilities for the quantitative study of quantum chromodynamics inaccessible by accelerator. The isotopic open of a band - gap in graphene proves that mass is created in massless fermions (leptons) in graphene by the strong nuclear interaction. The uniqueness of the isotope effect in the study of elementary particles dynamics in nuclear physics is emphasized.

References

1. Plekhanov VG (2021) Hadron - Lepton Interaction. LAMBERT Academic Publishing, Germany.
2. Perkins DH (2000) Introduction to High Energy Physics. CUP, Cambridge.
3. Cottingham WN, Greenwood DA (2007) An Introduction to the Standard Model of Particle Physics. CUP, Cambridge.
4. Griffiths G (2008) Introduction to Elementary Particles. Wiley - VCH, Weinheim.
5. Henley EM, Garcia A (2007) Subatomic Physics. World Scientific Publishing Co., Singapore.
6. Plekhanov VG, Buitrago JG (2019) Evidence of residual strong interaction in nuclear atomic level via isotopic shift in LiH - LiD crystals. Prog. Phys 15: 68-71.
7. Dee PI (1932) Attempts to detect the interaction of neutrons with electrons. Proc. Roy. Soc. (London) A136: 727-736.
8. Chadwick J (1932) The existence of a neutron. Proc. Roy. Soc. (London) A136: 692-708.
9. Aronberg (1918) Astrophys. J., 47: 96.
10. Condon EU (1936) Note on electron - neutron interaction. Phys. Rev 49: 459-461.
11. Striganov AP, Donzov Ju.P (1955) Isotope effect in atomic spectra. Uspekhi Fiz. Nauk (Moscow) 55: 315-330.
12. Foldy LL (1952) The electromagnetic properties of Dirac particles. Phys. Rev 87: 688-696.
13. Darwin CG (1928) the wave equations of electron. Proc. Roy. Soc. (London) A118: 654-680.
14. Bache J, Champeau R-J (1976) Recent progress in the theory of atomic isotope shift. Advances in At. Molec. Phys 12: 39-86.
15. Foldy LL (1958) Neutron - electron interaction. Rev. Mod. Phys 30: 471-481.
16. Mitsyna LV, Nikovenko VG, Parzhitski SS, et al., Extraction of the neutron - electron scattering length. Eur. Phys. J C40: 473-482.
17. Yukawa Y (1935) On the interaction of elementary particles. Proc. Phys. Math. Soc 17: 48-57.
18. King WH (1984) Isotope Shifts in Atomic Spectra Plenum Press. New York - London.
19. Plekhanov VG (2018) A possible signature of neutron quarks - leptons via gluon interaction in solids. Proc. 21th Int. Conf. Cond. Mat. Nucl. Sci., Fort collins, Colorado, USA.
20. Plekhanov VG (2018) Macroscopic manifestation of the strong nuclear interaction in the optical spectra of solids. Proc. 25 ISINN, Dubna, Russia 49-56.
21. Field JE (1982) The Properties of Natural and Synthetic Diamond (Academic Press, New York).
22. Plekhanov VG (2012) Isotope effect renormalization of the energy of electrons by strong nuclear interaction. Deposit in VINITI (Moscow) 13: N202 - B2012.
23. Plekhanov VG (2023) Solid - State Manifestation of Quantum Chromodynamics. Hadronic Journal 46: 359-457.
24. Boos EE (2022) The SMEET formalism: the basis for find in deviations from the Standard Model. Phys. - Uspekhi 65: 653-678.
25. Ioffe BL (2001) Chiral effective theory of strong interaction. Phys. - Uspekhi 44: 1211-1228.
26. Ioffe BL (2006) The origin of mass and experiments on high - energy particle accelerators. Phys. - Uspekhi 176: 1103-1104.
27. Karshenboim SG (2017) Constraints on a long - range spin - independent interaction from precision atomic physics. Phys. Rev. D 82: 073003-073005.
28. Delaunay C, Soreq Y (2017) Probing new physics with isotope shift spectroscopy. Phys. Rev. D 96: 115002-115006.
29. Delaunay C, Ozer R, Perez G (2017) Probing atomic Higgs - like forces at the precision frontier. Phys. Rev. D 96: 093001-093007.
30. Berengut JC, Budker D, Delaunay C (2018) Probing new long - range interactions by isotope shift spectroscopy. Phys. Rev. Lett 130: 091801-091807
31. Frugiuele C, Fuchs E, Perez G (2017) Constraining new physics models with isotope shift spectroscopy. Phys. Rev. D 96: 0150117-0150211.

32. Flambaum VV, Geddes AJ, Viatkina AV (2018) Isotope shift, non - linearity of King plots and the search for new particles. Phys. Rev. A 97: 032510.
33. Dzuba VA, Flambaum VV (2025) Using the Th III ion for a nuclear clock and searches for new physics. Phys. Rev. A 111: 053109.
34. Breit G (1958) Theory of isotope shift. Rev. Mod. Phys 30: 507-516.
35. Plekhanov VG (1996) Experimental manifestation of the effect of disorder on exciton binding energy in mixed crystals. Phys. Rev. B 53: 958-9561.
36. Plekhanov VG (2021) Experimental study of the long - range quark - lepton interaction in solids. Understanding Quarks, Chapter 1, Nova Science Publishing, Inc., New York.
37. Plekhanov VG (2005) Elementary excitations in isotope - mixed crystals. Phys. Reports 410: 1-235.
38. Plekhanov VG (2004) Giant Isotope Effects in Solids Stefan University Press. La Jola, CA.
39. Plekhanov VG (1997) Isotopic and disorder effects in large exciton spectroscopy. Phys Uspekhi 167: 577-604.
40. Knox RS (1963) Theory of Excitons Academic Press. New York - London.
41. Dammak H, Antoshchenkova E, Hayoum E (2012) Isotope effects in lithium hydride and lithium deuteride crystals by molecular stimulations. J. Phys.: Condens. Matter 24: 435402-435406.
42. Zimmerman WB (1972) Lattice constant dependence on isotope composition in the 7Li(H, D) system. Phys. Rev. B 5: 4704-4707.
43. Mohr P, Newell D, Taylor B (2016) CODATA recommended values of the fundamental physical constants 2014. Rev. Mod. Phys 88: 035009-035011.
44. Pekar SI (1954) Investigations into the electron theory of crystals, Academy-Verlag, Berlin.
45. Born M, Huang K (1954) Dynamical Theory of Crystal Lattices Clarendon. Oxford.
46. Plekhanov VG (2019) Measurements of the wide value range strong nuclear interaction coupling constant, SSRG Intern. J. Appl. Phys 6: 32-37.
47. Born M (1989) Atomic Physics. Dover Publication Inc., New York.
48. Harrison WA (1980) Electronic Structure and Properties of Solids W.H. Freeman and Company. San Francisco.
49. Alexandrov Yu F (1982) Fundamental Properties of the Neutron Energoizdat. Moscow.
50. Plekhanov VG (2018) Phenomenology of the origin of isotope effect. Phys. Sci. Int. J 18: 1-11.
51. Griffiths DJ (1982) Hyperfine splitting in the ground state of hydrogen. Am. J. Phys. 50: 698-703.
52. Deur A, Brodsky SJ, Teramond GF (2016) The QCD running coupling constant. Prog. Part. Nucl. Phys 90: 1-74.
53. Lederer CM, Shirley VS (1978) Table of Isotopes. (Wiley, New York).
54. Shirokov Ju.M, Judin NP (1980) Nuclear Physics (Science, Moscow).
55. Plekhanov VG (2018) Introduction to Isotopic Materials Science. (Springer, Heidelberg).
56. Ferrari AC, Bonaccorso F, Falko V, Novoselov KS, Roche S, et al. (2014) Science and technology road map for graphene, related two - dimensional crystals, and hybrid systems. Nanoscale 7: 4598-4810.
57. Harrison WA (1964) Electronic Structure and Properties of Solids (W.F. Freeman and Co., San Fransicko).
58. Clark CD, Dean PJ, Harris PV (1964) Intrinsic edge absorption in diamond. Proc. Roy. Soc. (London) A 277: 312-329.
59. Collins AT, Lawson SC, Kanda K (1990) Indirect energy gap of 13C. Phys. Rev. Lett 65: 891-893.
60. Ruf T, Cardona M, Pavone P, Wahl S, Thonke K, et al. (1998) Cathodoluminescence investigation of isotope effect in diamond. Solid State Commun 105: 311-316.
61. Watanabe H, Koretsune T, Nakashina S, Saito S, Shikata S, et al. (2013) Isotope composition dependence of the band - gap energy in diamond. Phys. Rev. B 88: 205420-205425.
62. Cardona M, Thewalt MLW (2005) Isotope effects on the optical spectra of semiconductors. Rev. Mod. Phys 77: 1173-1224.
63. Agekyan VF, Asnin VM, Kryukov AM (1989) Isotope effect in germanium. Fiz. Tverd. Tela (St. Petersburg) 31: 101-104.
64. Bilz H, Kress W (1979) Phonon Dispersion Relation in Insulators (Springer - Verlag, Berlin - Heidelberg).
65. Hanzawa H, Umemura N, Nisida Y, Kanda H, Okada M, et al. (1996) Direct effects of nitrogen impurities, and 13C isotope composition on the Raman spectrum 1b diamond. Phys. Rev. B 54: 3793-3799.
66. Chrenko RM (1988) 13C-doped diamond: Raman spectra. J. Appl. Phys 63: 5873-5875.
67. Spitzer J, Etchegoin P, Cardona M, Anthony TR, Banholzer WF, et al. (1992) Isotopic-disorder induced Raman scattering in diamond. Solid State Commun 88: 509-514.
68. Hass KC, Tamor MA, Anthony TR, Banholzer WF (1992) Lattice dynamics and Raman spectra of isotopically mixed diamond. Phys. Rev. B 45: 7171-7182.
69. Ramdas AK, Rodriguez S (1999) Lattice vibrations and electronic excitation in isotopically controlled diamonds. phys. stat. sol. (b) 215: 71-80.
70. Widule F, Ruf T, Konuma M, Silier I, Cardona M, et al. (2001) Isotope effects in elemental semiconductors: a Raman study of silicon. Solid State Commun 118: 1-23.
71. Wallace PR (1947) The band theory of graphite. Phys. Rev 71: 622-629.
72. Han MY, Ozyilmaz B, Zhang Y, Kim P (2007) Energy band - gap engineering of graphene nanoribbons. Phys. Rev. Lett 98: 206805-206814.
73. Ponomarenko LA, Schedin F, Katsnelson MI, Hill EW, Novoselov KS, et al. (2008) Chaotic Dirac billiard in graphene quantum dots. Science 320: 356-358.
74. Savchenko A (2009) Transforming graphene. Science 323: 589-590.
75. Elias DC, Nair RR, Mohiuddin TMG, Morozov SV, Blake P, et al. (2009) Control of graphene properties by reversible hydrogenation: Evidence for graphene. ibid 323: 610-613.
76. Plekhanov VG (2011) Nuclear technology creation the quantum dots in graphene. Transactions Humanitar Institute, Tallinn 66-70.
77. Plekhanov VG (2015) (unpublished results).See special issue Nature (2009) June 11 (2009).
78. Mak KF, Lui CH, Heinz TF (2009) Observation of an

electric - field - induced band gap in bilayer graphene by infrared spectroscopy. Phys. Rev. Lett 102: 256405-256414.
79. Castro EV, Novoselov KS, Morozov SV, Peres NMR, Lopes dos Santos JMB, et al. (2007) Biased bilayer graphene: semiconductor with a gap tunable by the electric field effect. ibid 99: 216802-216814.
80. Prawer S, Nemanich RJ (2004) Raman spectroscopy of diamond and doped diamond. Phil. Transac. R. Soc. (London) 362: 2537-2565.
81. Dresselhaus MS, Dresselhaus G, Hofman M (2008) Raman spectroscopy as a probe of graphene and carbon nanotubes. ibid 366: 231-236.
82. Casiraghi C, Hartschuh A, Qian H, Piscanec S, Georgi C, et al. (2009) Raman spectroscopy of graphene edges. Nano Lett 9: 1433-1441.
83. Sh. Chen, Wu Q, Mishra C, Kang J, Zhang H, et al. (2012) Thermal properties of isotopically engineered graphene. Nature Mater 11: 203-207.
84. Ferrari A (2007) Raman spectroscopy of graphene and graphite: Disorder, electron - phonon coupling, doping and nonadiabatic effects. Solid State Commun 143: 47-57.
85. Huang M, Yan H, Chen C, Song D, Heinz TF, et al. (2009) Raman spectroscopy of graphene under uniaxial stress: phonon softening and determination of crystallographic orientation. Proc. Natl. Acad. Sci 106: 7304-7315.
86. Zh.H. Ni, Yu T, Lu YH, Wang YY, Feng YP, et al. (2009) Uniaxial strain on graphene: Raman spectroscopy study and band - gap opening. ACS Nano 3: 483-492.
87. Mohiuddin TM, Lombarto A, Nair RR, Bonetti A, Savini G, et al. (2009) Uniaxial strain in graphene by Raman spectroscopy: G peak splitting, Grűneisen parameter and sample orientation. Phys. Rev. B 79: 205433-205438.
88. Kun CK, Yu L Q, Bo T, ZhiYi H, Lin W, et al. (2014) Isotope effect of the phonons means free path in graphene by micro - Raman measurement. Science China, Phys., Mech. and Astro 57: 1817-1821.
89. Plekhanov VG (2020) Renormalization of the band - gap by isotope in graphene. Nano Technol. and Nano Sci. J 3: 121-130.
90. Sofo JO, Chauhari AS, Barber A (2007) Graphanr: A two - dimensional hydrocarbon. Phys. Rev. B 75: 153401-153414.
91. Huang M, Yan H, Chen C, Song D, Heinz TF, et el. (2009) Raman spectroscopy of graphene under uniaxial stress: phonon softening and determination of crystallographic orientation. Proc. Natl. Acad. Sci 106: 7304-7315.
92. Nair RR, Ren WC, Riaz J, et al. (2010) Fluorographene two - dimensional counterpart of Teflon. Small 6: 2877-2884.
93. Farjam M, Rafii-Tabar H (2009) Comment on “Band structure engineering of graphene by strain: First - principles calculations”. Phys. Rev. B 80: 167401-167413.
94. Herrero CP, Ramirez R (2020) Isotopic effect in structural properties of graphene. Eur. Phys. J. B 93: 146-158.
95. Ken-ichi Sasaki (2018) Massive Dirac fermions signal in Raman spectrum of graphene. Phys. Rev. B 97: 115413-115416.
96. Roberts C.D (2015) Hadron physics and QCD: Just the basic facts. J. Phys.: Conf. Ser 630: 012051.
97. Roberts CD (2020) Empirical consequences of emergent mass. Symmetry 12: 1468-1506.